MAX '91

AN ADVANCED PAYLOAD FOR THE EXPLORATION OF HIGH ENERGY PROCESSES ON THE ACTIVE SUN

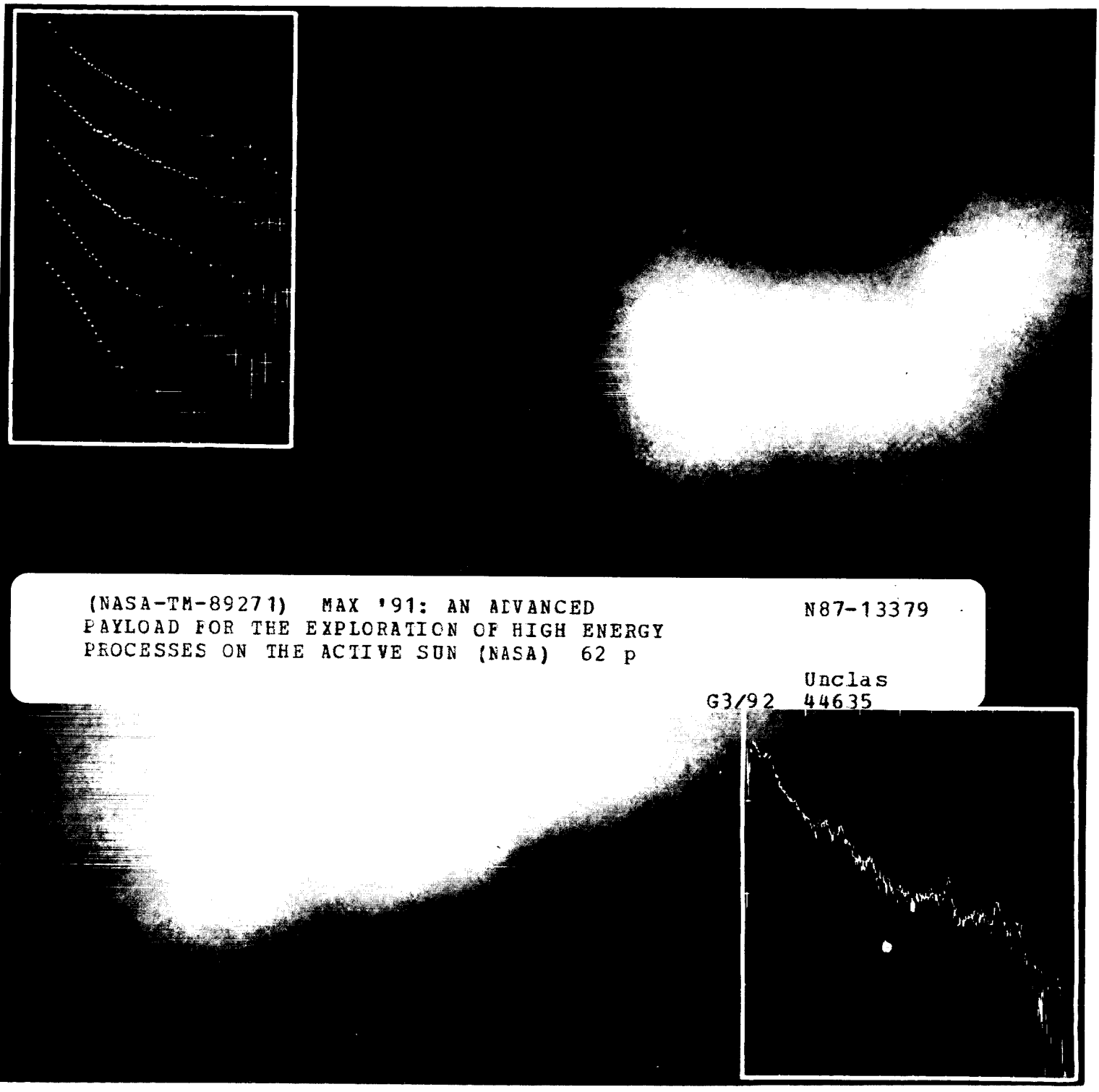

Report of the MAX '91 Science Study Committee commissioned by the National Aeronautics and Space Administration.

June 1986

Front Cover

An Hα photograph of a flaring region shown in red with a 15 GHz microwave image of the flaring loops superimposed in blue. The Hα photograph was obtained at Big Bear Solar Observatory, and the microwave image was obtained using Fourier-transform techniques at the Very Large Array. The two images were obtained nearly simultaneously during a flare on 23 March 1980; they cover a 30-arcsecond ($2 \cdot 2 \times 10^4$ km) square on the solar surface, and the microwave image has an angular resolution of 0·5 arcseconds. The white areas show the positions of the most intense Hα emission, probably at the footpoints of magnetic loops, while the blue areas show the presence of $\geq$100 keV electrons in two loops joining the two bright Hα regions. Simultaneous hard X-ray and γ-ray images with arcsecond resolution that could be obtained with the **MAX '91** payload would allow the energy spectrum and number of high-energy electrons to be determined. This information would allow the magnetic field strength in the loop to be estimated from the microwave intensity. Observations of temporal variations in the X-ray spatial structure on subsecond to second timescales will enable us to discriminate between different possible flare models, as discussed in the report.

Top left. High-resolution spectra of the bremsstrahlung X-ray continuum emission between 15 and 300 keV measured during the impulsive phase of a solar flare on 27 June 1980. The observations were made with a balloon-borne array of cooled germanium detectors with keV energy resolution, similar to those proposed for the **MAX '91** payload. These observations allowed, for the first time, an accurate measurement of the extremely steep thermal spectrum that becomes increasingly dominant at lower energies. This allows the temperature of the emitting plasma to be accurately determined (34×10^6 K in this case) and provides for a clear separation of this thermal component from the higher-energy component with its much flatter spectrum. Further details are given in Section 2.1 of the report.

Bottom right. γ-Ray spectrum of a flare on 27 April 1981, covering the energy range from 300 keV to 10 MeV. The spectrum was obtained with the Gamma-Ray Spectrometer on the Solar Maximum Mission (**SMM**). It shows several peaks from nuclear γ-ray lines superimposed on the bremsstrahlung continuum and unresolved line emission. The smooth curve represents a theoretically calculated spectrum. Elemental abundances of the ambient gas in the region where the accelerated protons interact have been calculated by fitting such theoretical spectra to the data. The high-purity germanium detectors proposed for the γ-ray spectrometer in the **MAX '91** payload have an energy resolution 40 to 100 times higher than that of the NaI(Tl) crystals used for the **SMM** spectrometer. Thus, it will be possible for the first time to measure the widths and shapes of many of the nuclear γ-ray lines. Observations with such a high-resolution spectrometer would herald the first true γ-ray spectroscopy and provide information on the number, energy spectrum, and possible beaming of high-energy particles, and on the elemental composition of the target. Further details are given in Section 2.1.

MAX '91

AN ADVANCED PAYLOAD FOR THE EXPLORATION OF HIGH-ENERGY PROCESSES ON THE ACTIVE SUN

Preface

This report gives the results of a NASA science working group established to study a follow-on to the Solar Maximum Mission. A complement of instruments is suggested, with the primary objective of studying the physics of energetic processes in cosmic plasmas by observing high-energy phenomena in solar flares. High-quality flare observations will be possible with these instruments during the next peak in solar activity expected to last from 1990 through at least 1995.

This science working group is the second with the name **MAX '91**; the first was chaired by Loren Acton in 1984. The present group met a total of six times between February 1985 and February 1986. We list below the names and affiliations of members of the study group and of other people who have made significant contributions to the work of the committee.

Brian Dennis/GSFC–Chairperson
Edward Chupp/UNH
Carol Jo Crannell/GSFC
George Doschek/NRL
Hugh Hudson/UCSD
Gordon Hurford/CIT
Sharad Kane/UCB
Robert Lin/UCB
Thomas Prince/CIT
Reuven Ramaty/GSFC
Gerald Share/NRL
Einar Tandberg-Hanssen/MSFC

Additional Contributors

David Bohlin/NASA-HQ
Marilyn Bruner/Lockheed
Frank Cepollina/GSFC
Tom Cline/GSFC
Len Culhane/MSSL, UK
Joseph Dabbs/MSFC
John Davis/MSFC
Philip Dunphy/UNH
Gordon Emslie/UAH
David Forrest/UNH
Tom Gergely/NASA-HQ
Leon Golub/CFA
Richard Hoover/MSFC
Kevin Hurley/CESR,
Toulouse, France
Stuart Jordan/GSFC
Gottfried Kanbach/Max Plank,
Garching, FRG
Alan Kiplinger/GSFC
Jim Lemen/MSSL, UK
Eugene Maier/GSFC
Robert Novick/Columbia
Larry Orwig/GSFC
George Simnett/U Birmingham, UK
Sabatino Sofia/Yale
Daniel Spicer/GSFC
Keith Strong/Lockheed
Roger Thomas/GSFC
Frank van Beek/Delft, Netherlands
Arthur Walker/Stanford
Peter Willmore/U Birmingham, UK
Richard Willson/JPL
Kent Wood/NRL

NASA-HQ Study Program Scientist: David Bohlin

SUMMARY

The primary objective of **MAX '91** is to study energetic processes in cosmic plasmas by observing high-energy phenomena in solar flares. These processes, which are of general astrophysical importance, include the following:

• Energy Release •Particle Acceleration •Energy Transport

Results from comprehensive observing programs conducted during the last solar cycle have demonstrated the great scientific potential of high-energy emissions for addressing these central physical processes. Consequently, a payload optimized for observations of high-energy solar flare phenomena is suggested for **MAX '91**. It consists of the following four specific instruments:

- A Fourier-transform X-ray and γ-ray imager covering the energy range from a few keV to 1 MeV with arcsecond spatial resolution.
- A cooled germanium X-ray and γ-ray spectrometer with keV spectral resolution covering the energy range from 10 keV to 50 MeV. The bismuth-germanate active anticoincidence shield of this instrument also acts as a γ-ray and neutron spectrometer to energies as high as 1 GeV.
- Bragg spectrometers with high spectral resolution at wavelengths between 1 and 9 Å.
- A soft X-ray, EUV, or UV imaging instrument with arcsecond spatial resolution.

Such a payload will provide the following major advances over previous results:

- The first ever imaging of hard X-rays and γ-rays above 40 keV.
- Hard X-ray and γ-ray imaging above 5 keV with improved sensitivity, spatial resolution, and temporal resolution to clearly resolve flaring magnetic loops.
- High-resolution γ-ray spectroscopy to resolve nuclear lines and determine line shapes.
- High-resolution X-ray spectroscopy to measure steep spectra from superhot ($>3 \times 10^7$ K) plasma.
- Neutron and γ-ray spectroscopy at energies from 10 MeV to 1 GeV.
- Soft X-ray, EUV, or UV images to provide plasma diagnostics and spatial distributions before, during, and after flares.
- High-sensitivity soft X-ray spectroscopy to determine plasma parameters, particularly those relating to upflows and turbulence during the early phases of flares.
- Complementary measurements of elemental abundances in the solar atmosphere from γ-ray and soft X-ray spectroscopy.

An already existing Multimission Modular Spacecraft or any similar three-axis-stabilized spacecraft could be used for **MAX '91**. Ideally, the payload would be placed in orbit in time for the next maximum in solar activity, expected to occur sometime between 1990 and 1992. High-quality flare observations will be possible through 1995. Unique observations of discrete and diffuse cosmic X-ray and γ-ray sources also could be obtained with this payload.

Table of Contents

Table of Contents (continued)

Appendixes

Figures

Tables

1. INTRODUCTION

The ability to release energy impulsively and accelerate particles to high energies is a common characteristic of cosmic plasmas at many sites throughout the universe, ranging from magnetospheres to active galactic nuclei. These high-energy processes play a central role in the overall physics of the system at each site where they are observed. The detailed understanding of these processes is one of the major goals of astrophysics, but in essentially all cases, we are only just beginning to perceive the basic physics.

Nowhere can one pursue the study of this basic physics better than in the active Sun, where solar flares are the direct result of impulsive energy release and particle acceleration. The acceleration of electrons to high energies is revealed by the hard X-ray and γ-ray bremsstrahlung, while the acceleration of protons to even higher energies is revealed by the nuclear γ-ray and neutron emissions. The fact that these accelerated particles may contain a major fraction of all the released flare energy is evidence for the fundamental role of the high-energy plasma processes. In addition, many lower-energy phenomena, some of which are the direct consequence of interactions of the accelerated particles, are also observed. It is the opportunity provided by solar flares to observe in detail the multitude of interwoven characteristics of high-energy plasmas that promises such a rich reward for the physicist and astrophysicist alike.

That this endeavor can indeed be profitably pursued in solar flares has been demonstrated by the pioneering observations carried out with instruments flown during the last active phase of the solar cycle (1978–1984) on the NASA Solar Maximum Mission (SMM), the Japanese **Hinotori** satellite, and other spacecraft. Many of the most important results from these observations were in the field of high-energy plasmas. These results include the following:

- The first hard X-ray images of solar flares. Such images reveal the location of energetic electrons that contain much of the impulsively released energy and suggest the existence of electron beams.
- Discovery of hard X-ray temporal variability on timescales of tens of milliseconds and of synchronization with UV emission to within 1 s. These observations provide the most severe constraints yet placed on the size, location, and nature of the energy release site.
- Detection of γ-ray lines and continuum from many flares. These observations demonstrate that the impulsive acceleration of protons to tens of MeV and electrons to relativistic energies is a basic property of the energy release process.
- Measurement of γ-ray and soft X-ray line spectra from solar flares. These are at present the most detailed astrophysical line spectra in these energy bands. Elemental abundances determined from them suggest significant abundance variations in the solar atmosphere.
- Direct observations of neutrons energetic enough to propagate to Earth before they decay and of γ-rays from π-meson decay. These observations demonstrate that impulsive proton acceleration extends to GeV energies.
- Discovery of "superhot" sources with temperatures in excess of 3×10^7 K. Because they cool very rapidly, these sources must be sustained by a continuous energy input. Therefore, they provide a direct record of the time history of the impulsive energy release.
- Observations of random mass motions and upflowing plasma at high temperature. These motions were found to be general characteristics of the soft-X-ray-emitting plasma and show that there is a very rapid and dynamic coupling between the initial energy release and the subsequently formed thermal plasma.

- Detection of a 154-day periodicity in the rate of occurrence of flares. This suggests a direct connection between high-energy solar activity and the internal dynamics of the Sun.

These discoveries were made with instruments that now seem crude in terms of spatial and spectral resolution. Nevertheless, they richly rewarded our intuition about the importance of high-energy observations of solar activity and point toward the potential scientific yield from a new program of observations utilizing state-of-the-art instrumentation with orders-of-magnitude improvements in capability.

This report describes the scientific objectives and the instrumentation for **MAX '91**, a mission optimized for the study of high-energy phenomena during the next phase of solar activity, which is expected to remain at a high level until at least 1995. Two high-energy instruments will have much-improved sensitivity and spatial, spectral, and temporal resolution over an energy range which extends from keV to GeV energies. The images from one of these instruments will be the first at photon energies above 40 keV. They will have arcsecond resolution and will be comparable in morphological detail to those obtained at microwave frequencies with the Very Large Array (VLA). The hard X-ray and γ-ray spectra from the other high-energy instrument will have sufficient energy resolution both to resolve the many nuclear lines observed with **SMM** and to separate the superhot component from the higher-energy hard X-ray continuum. Two other instruments observing at longer wavelengths, together with ground-based observatories, will define the structures in which the explosive high-energy phenomena take place and will reveal other direct manifestations of the impulsive energy release.

With the great improvements in resolution of these new instruments, we will be able to address the basic questions of high-energy plasma physics that are the driving scientific objectives of the proposed mission. For example, with arcsecond spatial resolution and subsecond temporal resolution matching the expected sizes and characteristic timescales associated with flare structures, we will be able to locate the regions of electron acceleration and follow the subsequent transport of the electrons. With keV spectral resolution, we will be able to resolve most individual γ-ray lines and measure their shapes and Doppler shifts. With such resolution, we will also be able to resolve the very steep X-ray spectrum of the superhot source and clearly separate it from the generally harder, power-law component at higher energies. With the combined data from all the instruments, we will, for the first time, be able to characterize all the fundamental high-energy aspects of solar flares, namely the energy release site, the accelerated particles, and the heated plasma.

In Section 2 we discuss the scientific rationale of the mission, the discoveries made during the last phase of solar activity, and the new observations and instrumental capabilities required. The **MAX '91** instruments are described in Section 3, with further details in the Appendixes. A possible technical approach is outlined in Section 4, and the implications of reusing an already existing Multimission Modular Spacecraft (MMS) to carry the **MAX '91** payload are discussed. Conclusions are given in Section 5.

We are indeed fortunate to be in a position in which great technological advances provide the orders-of-magnitude improvements necessary for a new generation of instruments to meet the challenge of the scientific requirements at a reasonable cost. Corresponding advances in other technologies such as computer networking will enable the full mobilization of scientific resources for analysis and coordinated interpretation of the data. Since solar activity is expected to peak in 1991, with high quality flare observations possible through at least 1995, we anticipate a high scientific yield from observations made with the proposed payload during this 5-year period.

2. SCIENTIFIC CONSIDERATIONS

2.1. Scientific Rationale

The relative proximity of the Sun makes it an ideal laboratory in which to investigate processes that occur in astrophysical plasmas. In particular, solar flares provide us with the opportunity to study high-energy processes in such plasmas. A major flare can liberate some 10^{32} ergs of magnetic energy over a period of minutes, involving the acceleration of relativistic electrons and ions on subsecond timescales. An understanding of the mechanisms by which energy is suddenly released in the flare has been a major challenge to physicists for several decades and remains so to this day. It is our intention that the proposed **MAX '91** payload address these areas of fundamental importance to astrophysics by providing definitive observations of radiation signatures of the energy release processes.

It has been known for some time that the source of flare energy is the solar magnetic field, but the processes that convert this energy into the observable flare manifestations are still not well understood. During the last solar maximum, a coordinated program aimed at addressing this problem was carried out with instruments on several satellites and many ground-based optical and radio observatories. The results of this effort made it clear that the flare energy release is fundamentally a high-energy phenomenon in which the acceleration of mildly relativistic electrons and ions is a central ingredient. It fact, it has been convincingly demonstrated that these particles contain a substantial fraction of all the released flare energy.

Magnetic loops in the solar atmosphere almost certainly play a dominant role in the flare process. A possible flare scenario, consistent with a wide variety of observational data, is illustrated in Figure 2.1. Here a single loop is shown, although much more complicated field geometries are usually present. As a result of the dissipation of magnetic energy (by an as yet ill-defined mechanism), electrons and protons are impulsively accelerated, probably in the coronal part of the loop. These particles subsequently propagate along the magnetic field lines and interact with the ambient gas in the legs of the loop and at the footpoints. As indicated in the figure, a variety of observable emissions are produced, but it is the hard X-rays, γ-rays, radio waves, and neutrons which are most closely linked to the acceleration process itself for the simple reason that these emissions must be produced before the accelerated particles lose their energy and thermalize in the ambient atmosphere. (The hard X-ray and γ-ray continuum is electron-ion bremsstrahlung, the γ-ray lines and neutrons are produced by nuclear reactions, and the microwaves are most probably gyrosynchrotron emission.)

The life history of a solar flare can be classified into an impulsive phase characterized by non-thermal emissions (hard X-rays, γ-rays, radio waves, and neutrons) and a gradual phase characterized by thermal emissions (soft X-ray, EUV, and optical). ***Since the thermalization of the particles and the equilibration of the radiation fields involve increases in entropy, it follows that the maximum information regarding the energy release itself can be obtained from observations of the flare manifestations that occur as close in time to the initial energy release as possible. Hard X-rays and γ-rays are among the earliest radiations emitted, and consequently their detailed study (particularly by imaging and spectroscopy) will provide the most valuable information on the crucial unsolved problems of energy release and particle acceleration.***

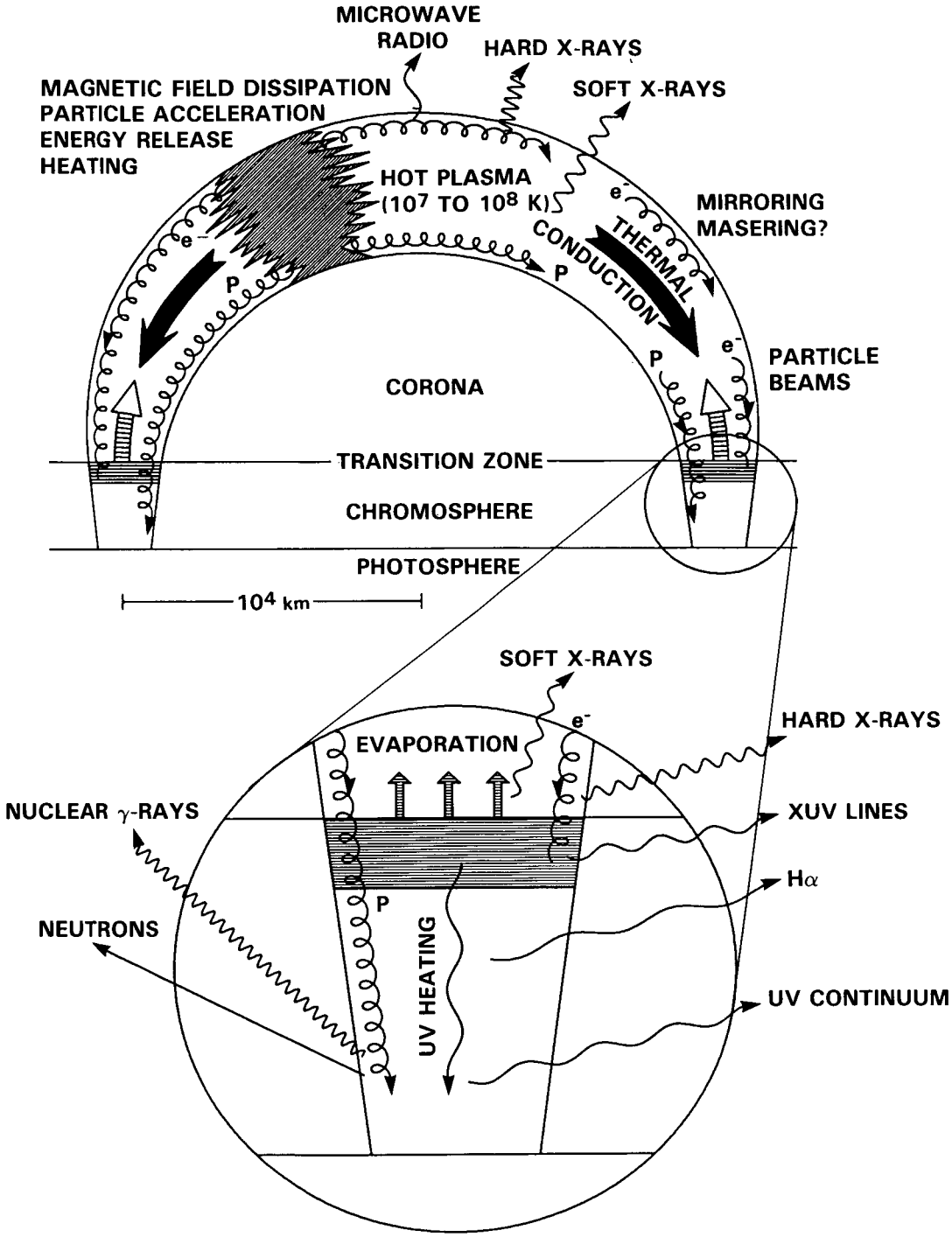

Figure 2.1. Schematic picture showing some of the physical processes believed to occur in a solar flare.

Radio emission also is prompt, and its observation provides a complementary picture of the high-energy processes. At metric and decimetric wavelengths, coherent plasma processes generate readily detectable emission from electrons on open field lines as well as from electrons in closed loops. At centimeter wavelengths, preflare emission can be used to measure magnetic field strengths in the low corona in which the energy release occurs; the impulsive phase emission gives information on electrons with energies above about 100 keV. The combination of microwave and hard X-ray imaging is especially powerful since the microwave emission is weighted by the magnetic field strength and the X-ray emission is weighted by the ambient density.

Related to the question of particle acceleration is the physics governing the transport of energetic particles throughout the solar atmosphere. Because of the high fluxes of particles and the correspondingly high ratio of the beam density to that of the background plasma, much of this physics involves the collective interaction of an accelerated ensemble of particles and is at present only sketchily understood in the astrophysical context. A thorough understanding of such processes, achieved through the interpretation of the radiation signatures (hard X-ray, γ-ray, soft X-ray, EUV, radio), will have application to broad fields of astrophysics and plasma physics.

Considerations of these issues clearly establish the study of energy release, particle acceleration, and energy transport in high-energy plasmas as the focal scientific objective of **MAX '91**. In addition, the advanced capabilities of this mission will allow us to address a variety of other solar objectives such as the study of elemental abundances, the observation of nonflaring solar activity, and the determination of preflare conditions. **MAX '91** will also be capable of making unique nonsolar observations. These include the imaging of hard X-ray sources with high angular resolution and the study of γ-ray lines with high-energy resolution from a variety of astrophysical sites.

In the rest of this section, we review the current status of the observations to establish the scientific context for **MAX '91**. First, we briefly outline the pioneering discoveries made during the last solar maximum and discuss some of the outstanding problem areas. Then, we discuss the future observations necessary to address the problems and to achieve the scientific objectives outlined above.

2.2. Discoveries Made During the Last Solar Maximum

▪ Evidence for Beams of Suprathermal Electrons

One of the long-standing models for solar flare hard X-ray production is the ***thick-target model*** in which beams of suprathermal electrons are accelerated in the corona and interact with ambient plasma in the flare loop to produce electron-proton bremsstrahlung (see Figure 2.1). Because of the Coulomb energy losses of these beamed electrons to ambient electrons, the bremsstrahlung process is quite inefficient, requiring that enormous amounts of energy reside in the accelerated electrons. Such large fluxes of electrons require either that some form of external driver such as a shock wave produce the acceleration or that a high degree of current filamentation exist within the acceleration region. An alternative model is the ***thermal model***, in which the bremsstrahlung-producing electrons form part of a thermal velocity distribution. Such a model can be considerably less taxing on the energy requirements for the electrons.

A clear discriminator between such models is the ***spatial structure of the hard X-ray bremsstrahlung source***. During some flares, the **SMM** Hard X-Ray Imaging Spectrometer (**HXIS**) and the Japanese **Hinotori** Solar X-Ray Telescope (**SXT**) obtained images which are consistent with a "footpoint" hard X-ray structure at energies around 20 keV, indicative of the non-thermal impact signature of the thick-target model. An example of such an image, showing bright patches in 16- to 30-keV X-rays associated with the footpoints of a magnetic loop structure, is shown in Figure 2.2.

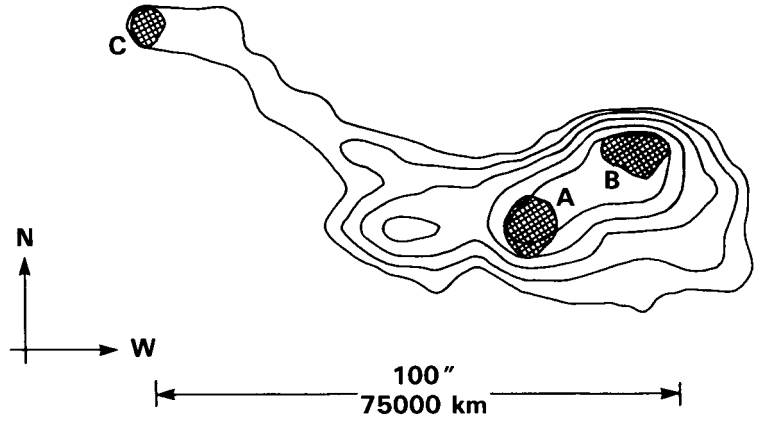

Figure 2.2. X-ray image of a solar flare on 5 November 1980 at 22:33 UT. The contour lines indicate the intensity of 3·5- to 8-keV soft X-rays, and the cross-hatched areas labeled A, B, and C show the bright patches of the 16- to 30-keV hard X-ray emission. These bright patches are believed to be at the footpoints of two interacting magnetic loops, one joining A and B and a larger one joining B and C.

Further evidence consistent with the thick-target model comes from stereoscopic views of ***behind-the-limb events*** seen from two different spacecraft. These observations show that the dominant component of high-energy ($\geq$ 100 keV) hard X-ray emission comes from low altitude, as expected from the thick-target model.

The ***close synchronism to within 1 s of hard X-ray and UV bursts***, observed with the **SMM** Hard X-Ray Burst Spectrometer (**HXRBS**) and Ultraviolet Spectrometer/ Polarimeter (**UVSP**), also points to the presence of non-thermal electron beams. The observations demonstrate a rapid energy transport mechanism whose associated velocity is inconsistent with a propagating thermal disturbance.

In addition, the ***impulsive enhancements in the chromospheric Fe Kα line***, observed simultaneously with some hard X-ray bursts, indicate the presence of precipitating electrons. This conclusion is also supported by studies of other impulsive phase observations such as the Hα line profile.

At energies above 10 MeV, evidence for electron beaming comes from the ***limb brightening*** apparent in Figure 2.3, in which the locations of all γ-ray events detected above 10 MeV with the SMM Gamma Ray Spectrometer (GRS) are plotted on the solar disk. It is clear that every event originated close to the limb, implying that the radiating particles, most probably relativistic electrons, are strongly beamed downward.

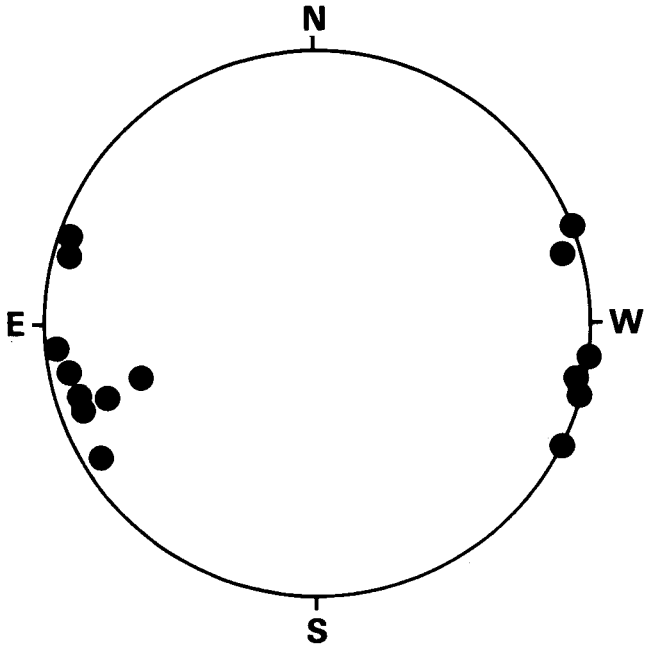

Figure 2.3. Limb brightening of solar flares detected in γ-rays above 10 MeV. The points show the locations on the solar disk of all flares detected with the SMM-GRS at energies above 10 MeV.

- **Prompt Acceleration of Protons**

Observations made with GRS show that γ-ray lines in the 4- to 8-MeV range, produced by ***nuclear de-excitations***, are emitted simultaneously with the hard X-ray bremsstrahlung continuum to within the 1-s timing accuracy of the data. Since the excited nuclei responsible for the emission of these lines are produced by high-energy proton impact, we conclude that ***impulsive proton acceleration*** is a ubiquitous and key feature of flare energy release. A comparison of the number of protons required to produce the γ-rays with the number of escaping protons observed directly in interplanetary space strongly suggests that the bulk of the protons are accelerated and remain trapped in closed magnetic structures, as indicated in Figure 2.1.

Observations of ***impulsive γ-rays produced by pion decay*** show that proton acceleration extends to energies as high as 1 GeV. This conclusion is also supported by SMM and ground-based observations of ejected neutrons. The neutron spectrum, and hence the proton spectrum, can be determined from the γ-ray and neutron time profiles and the neutron time of flight to the detector in Earth orbit. An example of the neutron observations is shown in Figure 2.4, where the SMM results are combined with ground-based neutron monitor observations and indirect estimates based on the measured proton fluxes resulting from the decay of the neutrons in interplanetary space. The detection of a neutron signal only about 100 s after the peak of the impulsive phase implies that neutrons, and hence protons, of at least 700 MeV were produced within a few tens of seconds of this peak time. The observed ratio of neutrons and γ-ray fluxes, as well as the ratios of various γ-ray line fluxes, provide information on the proton energy spectrum at the Sun that cannot be obtained in any other way.

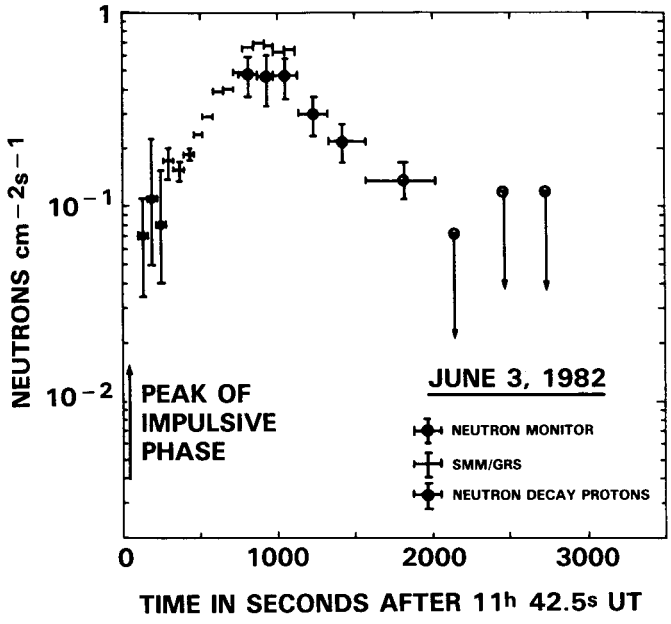

Figure 2.4. Direct observations of the solar neutron flux made with GRS plotted as a function of time after the impulsive phase of the flare on 3 June 1982. The neutron fluxes determined from neutron monitor observations and from measurements of interplanetry protons are also shown.

The observations of ***energetic solar particles in the interplanetary medium*** indicate that, for many flares, a separate but related acceleration process, probably due to the passage of ***shock waves*** through open magnetic structures in the high corona, is the source of most of the escaping particles. The γ-ray line production efficiency for this acceleration is probably lower than that for the impulsive acceleration in closed magnetic structures, but the high sensitivity of future instruments would enable γ-rays and neutrons to be detected from this acceleration phase as well.

- **Element Abundance**

The γ-ray spectra obtained with **GRS** show many individual lines, as seen in Figure 2.5. Spectra such as this provide unique information on the ***relative abundance of chemical elements*** at the γ-ray production site, most probably in the chromosphere. Such analysis suggests that the abundances of C and O relative to Mg, Si, and Fe are lower in the chromosphere than in the photosphere. This result implies a variation of chemical composition with space and time in the solar atmosphere and may even have implications for our knowledge of cosmic elemental abundances. In addition, unexplained ***abundance variations of Ca*** in flares have been found from the analysis of **SMM** soft X-ray spectra.

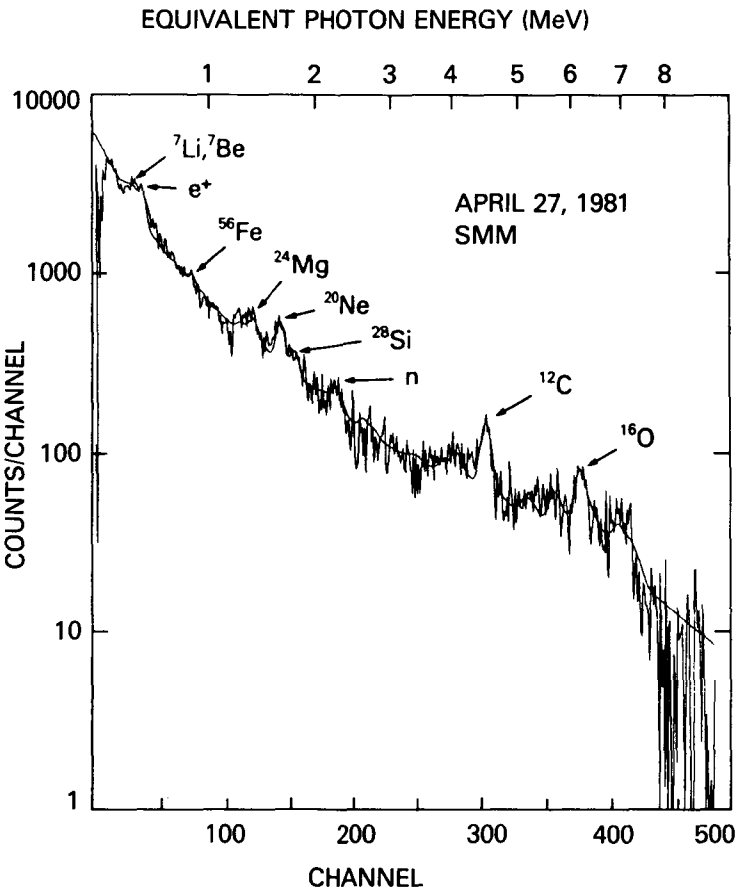

Figure 2.5. γ-Ray spectrum of a flare with several lines identified. The curve through the observations was obtained from a theoretical model with the relative elemental abundances chosen to give the best fit to the data.

▪ Rapid Fluctuations in Hard X-Ray and Microwave Bursts

Observations made with **HXRBS** show that many flares have ***subsecond variations in the hard X-ray flux***, with the shortest timescales observed being significantly ***below 100 ms***. An example of rapid fluctuations is shown in Figure 2.6. Fluctuations in the microwave flux on timescales down to 1 ms have also been reported. Observations of such rapid fluctuations demonstrate the need for X-ray imaging and spectroscopy with subsecond time resolution, so that the location and spectrum of individual bursts can be determined. The shortest timescales observed are comparable to the light travel time across sources with solar flare dimensions and therefore represent strong constraints on any flare model.

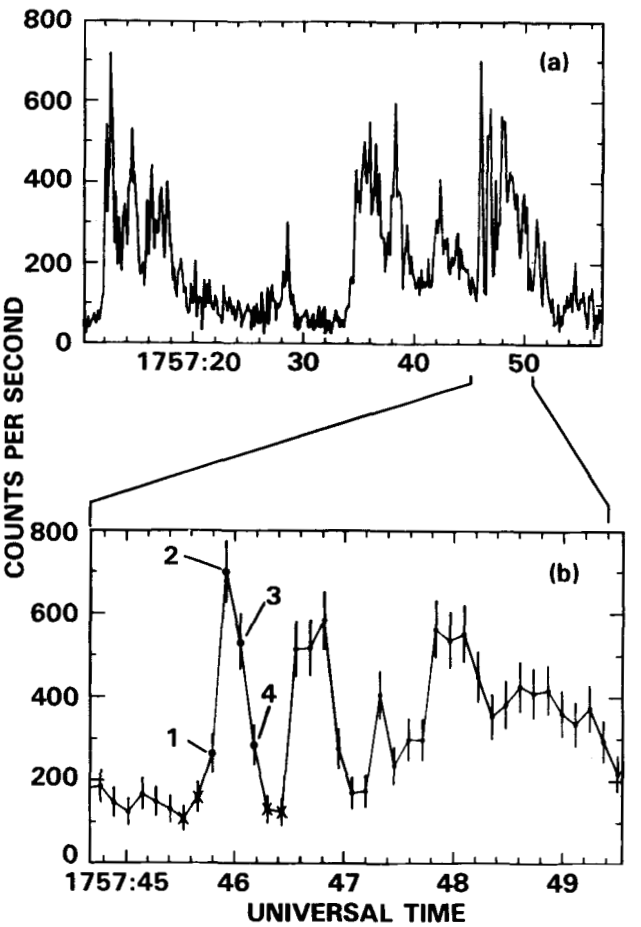

Figure 2.6. Hard X-ray time profiles (27 to 496 keV) of a solar flare which occurred on 10 May 1980. (a) A 40-s portion of the most impulsive phase of the event at a time resolution of 128 ms. (b) Expanded version of the region connected by lines to (a), with $\pm 1\sigma$ statistical error bars drawn vertically through each point. The numbered points show a single spike lasting no longer than 0·5 s.

▪ Chromospheric Evaporation

A feature of both the thermal and the non-thermal thick-target bombardment models is the rapid heating of chromospheric plasma, which subsequently expands and is driven upward into the corona. This process, or a variation of it, is commonly referred to as ***chromospheric evaporation***. It has been identified in a number of flare events through its characteristically ***blue-shifted component in soft X-ray spectral lines***. Intense turbulence during the impulsive phase is also revealed by the **broadening of the same spectral lines** (Figure 2.7).

Spatial images of such events obtained with **UVSP** show that the UV brightenings associated with multiple bursts in hard X-rays occur at different locations on the disk, suggesting that separate bursts are due to the energy release in different magnetic structures rather than to repeated flaring of the same loop.

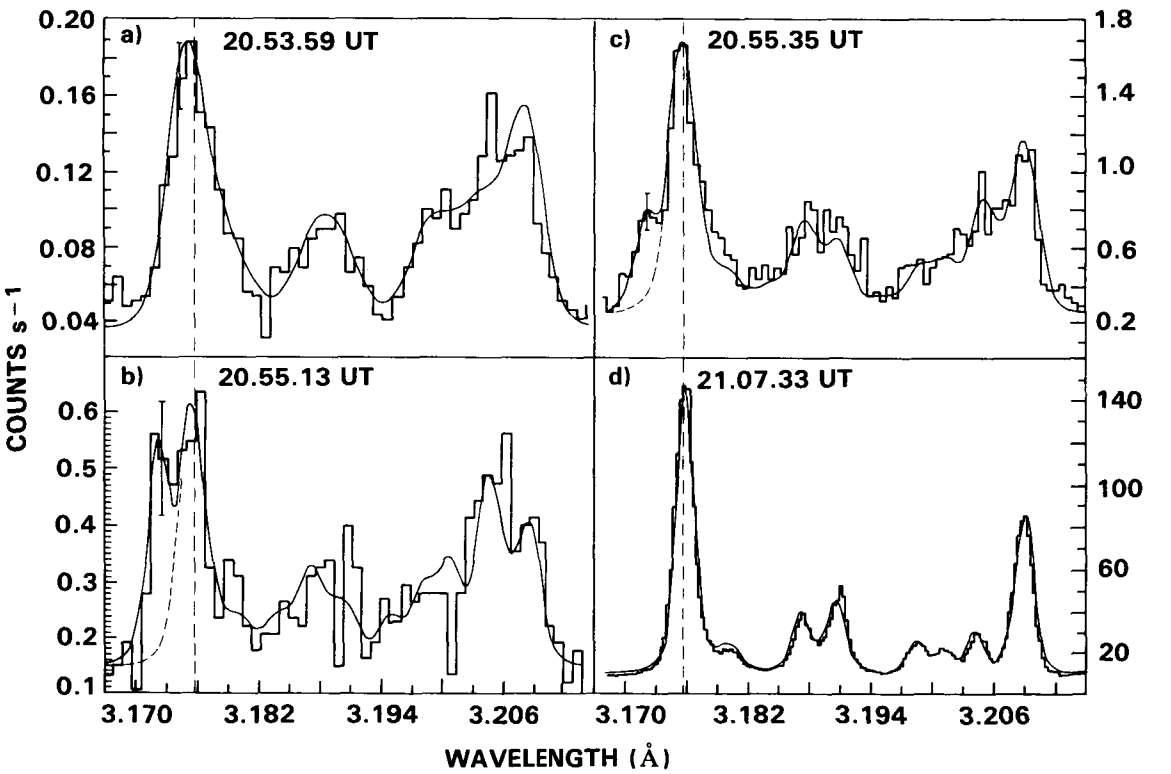

Figure 2.7. Sequence of Ca XIX spectra obtained at four times during the impulsive phase of the 21 May 1980 flare by BCS. Note that during the onset of the flare (a), the line profiles are broadened by mass motions. Later, during the impulsive phase (b) and (c), a blue-shifted component can be seen to the left of the peak centered on the broken line at 3.176Å, indicating an upflow of coronal material at velocities above 200 km s^{-1}. The last frame (d) shows the Ca XIX spectrum at the peak of the gradual phase when most of the mass motion effects are no longer apparent.

- **UV Continuum Enhancements**

A somewhat surprising result from the **HXRBS** and **UVSP** instruments is that the ***UV continuum shows impulsive behavior*** similar to that of UV lines and hard X-rays. This result is remarkable because the UV continuum is formed in relatively cool layers deep in the chromosphere (in the vicinity of the temperature minimum at $\leq 10^4$ K), as opposed to the UV lines, which are formed in the transition region above the chromosphere at about 10^5 K. Owing to the high density at the depths of the temperature minimum and the large amount of overlying chromospheric material, it is very difficult to invoke impulsive heating of these layers to explain the observations. Thus, the continuum must be excited by UV radiation from above. This important result shows that this ***UV line radiation has a significant effect on the energy balance of the lower atmosphere*** and is not simply a diagnostic of other physical processes, as had previously been thought.

- **Location of the Site of Particle Acceleration**

The accumulated evidence available to date suggests that ***particle acceleration takes place in the lower corona***. This assumption is built into most flare models, including the one shown in Figure 2.1.

The best evidence that electrons are accelerated in the corona at a density of about 10^9 cm^{-3} comes from correlated studies of ***hard X-ray and decimetric radio emissions***. These studies also suggest that the acceleration often occurs successively at different points in the corona. Measurements of ***metric radio bursts***, e.g., type II and type III bursts, show that electron acceleration also occurs in the high corona. Because of sensitivity limitations of current instruments, these high-altitude phenomena have essentially not been studied in hard X-rays and γ-rays.

Further evidence for ***coronal electron acceleration*** comes from microwave observations made with the **VLA**. The microwave emission produced as ***gyrosynchrotron radiation by mildly relativistic electrons*** spiraling in the magnetic field is seen to come primarily from near the top of flaring coronal loops. Furthermore, the microwave polarization observations indicate that electrons are present in both legs of the loop, centered about the loop top. Both of these results are consistent with a model in which the electrons are ***trapped inside the magnetic loop***. Although complicated by uncertainties in the magnetic field structure and in the electron velocity distribution, the simplest explanation of these observations is that the ***electrons are accelerated inside the trap*** itself near the loop top.

It is generally assumed that the protons and heavy ions that produce the γ-rays and neutrons are accelerated at the same location as the electrons, but direct observational evidence for this is not available.

- **Superhot Plasma**

Hard X-ray measurements made with high-energy resolution have revealed the presence of a thermal plasma with a temperature above 30×10^6 K, significantly hotter than the familiar thermal plasma at 10 to 20×10^6 K. This ***superhot plasma*** may have the highest temperature of any thermal source in flares. The hard X-ray spectra in Figure 2.8 show that its emission dominates at energies below about 30 keV from the time of maximum flux in the impulsive phase. The normal power-law hard X-ray component is apparent at high energies.

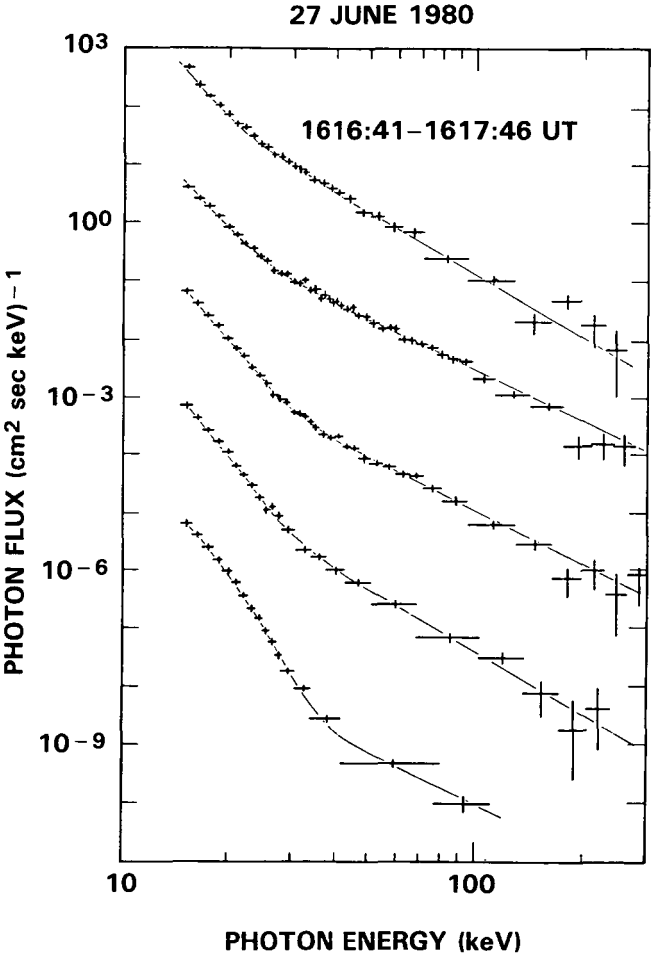

Figure 2.8. High-resolution hard X-ray energy spectra for a solar flare on 27 June 1980 obtained with an array of cooled germanium detectors flown on a high-altitude balloon. The vertical scale applies to the uppermost spectrum, with each succeeding spectrum offset downward by two decades. The component of the hard X-ray spectrum from the superhot plasma at 34×10^6 K is clearly seen below about 30 keV and becomes more dominant with time over the power-law component seen at higher energies.

This clear separation of the two components is impossible with scintillation detectors because of their much poorer energy resolution. The high-resolution spectra allow us to make a more reliable estimate of the ***total energy in the electrons*** responsible for the high energy component, since the extrapolation of its power-law spectrum to lower energies can now be made with the superhot spectrum subtracted out. In addition, the short conductive cooling times of such high-temperature sources require that they be sustained by a ***continuous energy input***, and so their behavior with time provides information on the time history of the energy release.

This superhot plasma appears to occur commonly in flares, suggesting that the imaging experiments on the **SMM** and **Hinotori**, with their limited energy range and sensitivity, may have been observing this superhot source rather than the higher-energy component.

- **154-Day Periodicity in Flare Activity**

Fourier analysis of γ-ray, hard X-ray, and microwave event-occurrence rates clearly indicates ***variability with a period of approximately 5 months***. The reason for this periodicity is not clear, and it will be of interest to see whether it persists through the 11-year solar cycle and to examine the comparative features of flares occurring at different phases. It has been suggested that this periodicity results from the ***interaction of various g-mode oscillations of the Sun***. If this is the case, it could reveal important parameters of the solar interior, such as the spin rate, that cannot be determined in any other way.

2.3. Required Observational Capabilities for MAX '91

The pioneering observations made during the last solar maximum show clearly that an understanding of the important physical processes in flares requires considerably more sophisticated observational capabilities. For example, while the hard X-ray imaging observations gave us our first glimpse of the sites of energetic electron interactions, they did not have the angular resolution, the time resolution, or the energy range to unambiguously specify which, if any, of the many quantitative flare models accurately describe the events. While the γ-ray spectroscopy observations provided the first detailed diagnostics of ion acceleration in flares, they did not have the energy resolution to explore the questions of line widths and Doppler shifts that are so important to the understanding of particle transport.

We now discuss these and other considerations in more detail. Although the emphasis is on observations that are motivated by, and build upon, previous discoveries, it would be very surprising indeed if the orders-of-magnitude improvements in observational capabilities discussed below did not themselves lead to additional new discoveries during the next solar maximum. Some possibilities are discussed in Section 2.5.

- **High angular resolution over an extended energy range**

The electrons responsible for high-energy X-rays and γ-rays have velocities approaching that of light, so that they traverse a typical solar flare with dimensions of about 10^9 cm ($\sim$ 15 arcseconds) in about 0.1 s. What is required, therefore, to study the temporal and spatial evolution of the bremsstrahlung-emitting electrons is a telescope with an angular resolution significantly better than 15 arcseconds and a time resolution less than or equal to 0.1 s. Further, the presence of superhot plasmas means that unambiguous analysis of the hard X-ray

bremsstrahlung from the accelerated non-thermal electrons must be carried out at X-ray energies in excess of 50 keV. In contrast to these requirements, the best angular resolution to date in hard X-rays is of order 10 arcseconds (**HXIS** and **SXT**), and then only up to moderate energies (30 to 40 keV) and with coarse time resolution ($\sim$ 10 s).

Spatial resolution of hard X-rays at the arcsecond level is desirable to contrast features within the flaring source. It will allow us to trace the interaction of the electrons with the ambient plasma and hence locate the acceleration site. With sufficient sensitivity, the evolution of the electron energy spectrum from point to point along the flare loop can be analyzed, providing a direct measurement of the plasma processes affecting the evolution of a relatively dense beam of suprathermal electrons. Spatial resolution also minimizes the difficulty of obtaining the injected electron spectrum from spatially integrated hard X-ray measurements and provides information on the processes that modify the electron spectrum throughout the source.

The interpretation of hard X-ray imaging observations is also aided by the fact that such emission is optically thin and depends only on the momentum distribution of the electrons and the ambient density. In this respect, their interpretation is more straightforward than that of microwaves, whose emission can be strongly dependent on the magnetic field and whose propagation can be more complex.

- **High spectral resolution**

The γ-ray results obtained with **GRS** show the existence of numerous lines in the γ-ray spectra of many flares. The lines, however, were not resolved and true spectroscopy in the sense of measuring line profiles was not possible. Germanium spectrometers have much better energy resolution than the NaI(T*l*) scintillator used as the **GRS** detector so that sensitive measurements can be made for the first time of line profiles and Doppler shifts. Such measurements are needed to address many of the focal physical questions discussed in Section 2.1, including the beaming of accelerated particles. For instance, line profiles give detailed information on the kinematics of energetic ion interactions and relate directly to the degree of anisotropy of the energetic particles. Doppler shifts provide direct information on the directivity of particle acceleration.

High-spectral-resolution measurements of the hard X-ray continuum are also needed to resolve the very steep spectra often present in flares. This is particularly true for measurements of the superhot electron component, which can be made only with high-resolution detectors such as germanium spectrometers.

Finally, high-spectral-resolution observations of γ-ray lines allow much more precise measurements of elemental abundances in the energetic particle interaction region. These measurements were limited during the last solar maximum by the inability to clearly separate the discrete lines of individual elements and isotopes.

- **Spectroscopy of high-energy neutrons and γ-rays**

During the previous solar maximum, neutrons and pion decay γ-rays were observed for the first time. The neutron energy spectrum, combined with the γ-ray spectrum from pions, provides the best tool for the study of the accelerated proton spectrum at high energies. To fully exploit this new diagnostic of the flare process, observations with higher sensitivity and improved energy resolution are required. The γ-rays must be measured with better energy

resolution and sensitivity than was done with **GRS** to separate the pion and electron-ion bremsstrahlung components at energies above about 20 MeV. Also, the neutron energies must be directly measured rather than deduced from the arrival time, since the latter method is subject to ambiguities when the neutrons are produced over extended time intervals.

- **Imaging and spectroscopy in the soft X-ray, EUV, and UV bands**

Knowledge of both the preflare conditions and the thermal response of the atmosphere to the release of the flare energy is necessary to correctly interpret the hard X-ray and γ-ray observations in terms of the overall flare phenomenon. Arcsecond imaging of the thermal plasma at temperatures between 10^4 and 2 x 10^7 K would provide the required information on the active-region structures involved in a flare. Such information is needed to determine what large-scale magnetic structures can lead to a flare and how these structures change and relax during and after the flare.

The X-Ray Polychromator (**XRP**) and **UVSP** provided some of the necessary plasma diagnostics (temperature, density, velocity) on **SMM**. For future missions, instruments with spatial and temporal resolutions similar to those of the high-energy instruments are required to image the thermal plasmas and to provide the required high-resolution spectroscopy. The technology is available and suitable atomic spectral lines exist to adequately cover the required temperature range in several different wavelength bands including soft X-rays, EUV, and UV. These low-energy observations would not only provide the necessary plasma parameters to place the high-energy observations in the context of the thermal flare, but also provide important complementary data on lower-energy flare processes. These capabilities are discussed further in Sections 3.3 and 3.4.

2.4. Required Instrumentation

After taking into account all of the considerations described above, it is clear that an ideal payload for future study of the impulsive-phase, high-energy phenomena in solar flare plasmas would include the following four instruments:

- A hard X-ray and γ-ray imaging spectrometer with high spatial resolution
- A hard X-ray and γ-ray spectrometer with high spectral resolution and neutron detection capability
- A soft X-ray spectrometer with high spectral resolution
- A low-energy imaging instrument in the soft X-ray, EUV, or UV band.

Instruments capable of achieving the required resolutions and sensitivities are now being developed for balloon or rocket flights, and versions suitable for space flight could be readied in time for the next solar maximum. The **MAX '91** payload described in Section 3 is made up of four such instruments. They all have high sensitivities, so that observations could be made with high time resolution even during the early impulsive phase of modest flares. When combined with ground-based radio and optical support, this payload will address all facets of the flare shown schematically in Figure 2.1.

An indication of the most favorable period for future flare observations with this payload can be obtained from Figure 2.9, which shows the hard X-ray and γ-ray flare rates for the last

solar cycle. This figure shows that between 200 and 2000 hard X-ray flares and 10 to 50 γ-ray flares were observed in any one year from 1980 to 1985. Furthermore, the largest γ-ray flare occurred in April 1984, 4 years after the sunspot maximum. Similarly, in the previous solar cycle, the largest γ-ray flares occurred about 3 years after sunspot maximum. Thus, with the very significant increase in sensitivity expected for the **MAX '91** instrumentation, an excellent set of hard X-ray and γ-ray flare observations can be expected through 1995.

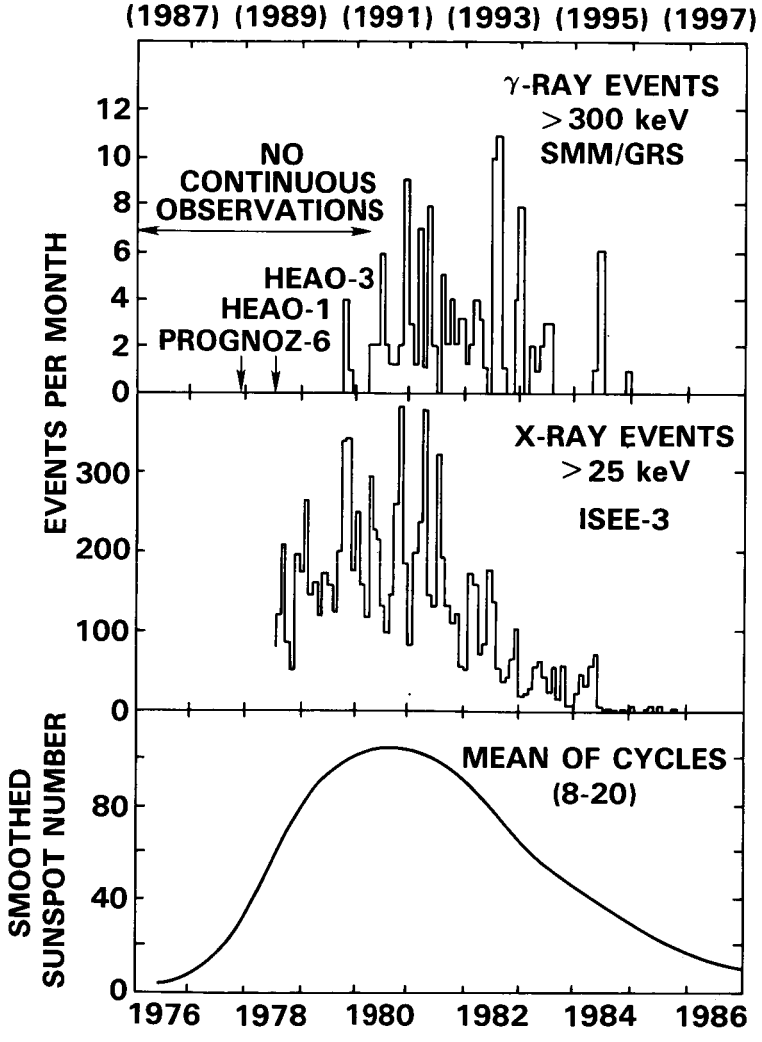

Figure 2.9. Rates of γ-ray and hard X-ray flares over the last 11-year solar cycle (Cycle 21). The years in parentheses on the upper scale show the corresponding phase of the next cycle. Also shown are the smoothed sunspot numbers averaged over Cycles 8 through 20. Note that hard X-ray and γ-ray flares were seen in significant numbers several years after the nominal maximum of Cycle 21, which was in December 1979.

2.5. Potential for New Solar Discoveries

The tremendous increase in sensitivity of the **MAX '91** instruments over that of previous instrumentation opens up an entirely new regime of solar hard X-ray and γ-ray phenomena for study. Some of the possible areas of discovery are listed below.

- **Microflares**

Solar hard X-ray bursts with 20-keV fluxes that are a factor of 10 to 100 times lower than those of typical small flares were discovered with a very-high-sensitivity detector on a balloon flight. At the time of the observations in 1980, these microflares were occurring about once every 5 min. The observations suggest that even very small transient releases of energy by the Sun may be primarily non-thermal in character. Furthermore, the energy released in these small bursts averaged over time might be a significant contributor to the heating of the active corona. Perhaps even soft X-ray bright points have significant non-thermal hard X-ray components. The **MAX '91** instruments should be able to provide both imaging and spectral measurements of microflares and detect them to significantly lower flux levels.

- **Shock acceleration in the high corona**

Observations of energetic solar flare particles escaping to the interplanetary medium indicate that these particles are accelerated in the quiet corona, most probably by the passage of shock waves. Furthermore, there are some flares, notably those on 4 August 1972 and 3 June 1982, in which the γ-ray emission was clearly delayed or extended well past the impulsive phase. Thus, an apparently separate but related acceleration of particles very likely occurs high in the corona. Galactic cosmic rays are believed to be accelerated by supernova shock waves, probably by the same physical mechanisms. Although the density in the high corona is very low and bremsstrahlung X-rays and nuclear γ-rays are both produced by collisions with the ambient plasma, the high sensitivity of the **MAX '91** instruments will allow this acceleration mechanism to be studied in detail.

- **Type III radio bursts and coronal flares**

A type III radio burst is the most common type of impulsive phenomenon occurring on the Sun. This radio emission has been shown to be produced by electrons of a few to about 100 keV as they escape from the Sun after an impulsive acceleration. Many, perhaps most, type III bursts have starting frequencies below about 100 MHz, implying heights of $>1R_{\odot}$. These flare-like impulsive acceleration events in the high corona are now known to be closely related to ^{3}He-rich events, impulsive particle events observed in interplanetary space which have an anomalously high abundance of the isotope ^{3}He, sometimes with the ^{3}He:^{4}He ratio > 1. High sensitivity imaging and spectral measurements could locate the acceleration region and provide clues to this highly selective acceleration mechanism.

Storage of energetic particles can occur in the high corona, where the ambient density is low and the lifetimes of the energetic particles are correspondingly long. Such storage may play a significant role in flare and particle acceleration processes. With the high-sensitivity instruments proposed for **MAX '91**, these stored particles can be directly detected and imaged via their bremsstrahlung and γ-ray emission.

2.6. Nonflaring Solar Activity

Complementary to the study of large active regions are studies of small-scale emerging magnetic flux, particularly in the form of X-ray bright points and ephemeral active regions. Large active regions represent only a small fraction of the total magnetic flux which emerges at the solar surface; the overall balance between large and small emerging regions is such that the total rate of magnetic flux emergence is nearly constant throughout the cycle. At present, we do not know the smallest scale size of flux emergence regions. The size spectrum must turn over at some point, and the improvement in spatial resolution obtainable with the **MAX '91** instrumentation could be used to determine this value.

One of the important objectives of active region studies is to determine the preflare conditions. Identification of the preflare magnetic configuration would constitute a major advance in our understanding of energy release processes in solar flares. Although the hot coronal flare plasma is known to exist in magnetic loops, it has not as yet been possible to identify the preflare magnetic configuration. It is probable, however, that the preflare configuration differs significantly from the configuration during the peak X-ray-emitting phase of flares. This is known from observations of erupting filaments and the dynamic activity coincident with the impulsive phase. Furthermore, it is known that, at least for some flares, there is an extended period of low-level heating just before the onset of the impulsive phase. It should be possible to detect this preflare heating and indentify magnetic structures that evolve into the dense plasma loops of the thermal coronal flare.

2.7. Capabilities for Cosmic Hard X-Ray and γ-Ray Astronomy

It is clear that the instruments required for the high-energy solar observations will also be very powerful for making observations of other cosmic sources.

- **The Hard X-Ray and γ-Ray Imager**

The **MAX '91** hard X-ray and γ-ray imager would complement other facilities such as the Gamma Ray Observatory (**GRO**) and the X-ray Timing Explorer (**XTE**) by adding the capabilities for high-sensitivity, moderate-resolution spectroscopy in crowded fields (e.g., the galactic center region) and imaging with very high angular resolution.

Among the possible imaging applications are surface brightness mapping of extended sources (such as the Crab Nebula), precise positioning of sources to identify counterparts, and imaging of crowded or confused fields. For example, the imager could be used to position the 511-keV source near the galactic center to an accuracy of about 1 arcsecond. The fine angular resolution could also be used with long integration times to isolate hard X-ray sources down to very low flux levels. This would permit extensive statistical studies on active galactic nuclei to be performed. Active-galactic nuclei with jets (e.g. Cen A and M87) could be imaged at high energies to determine the jet-to-nucleus ratio of the γ-ray and hard X-ray emission. Also, certain clusters of galaxies known to contain hard X-ray-emitting components could be imaged to localize and map those components.

- **The Hard X-Ray and Gamma Ray Spectrometer**

The **MAX '91** hard X-ray and γ-ray spectrometer would provide the high spectral resolution required for the detection and measurement of narrow lines and other sharp spectral features of astrophysical sources. This capability is not available with instrumentation on **GRO** or other approved spacecraft missions. This instrument is particularly well suited for spectroscopy of cosmic γ-ray bursts and other transients, in which gravitationally red-shifted positron annihilation and other nuclear γ-ray lines as well as narrow cyclotron line features have been observed.

The study of γ-ray lines emitted by the radioactive decay of unstable isotopes produced in explosive nucleosynthesis by supernovae and novae is another major objective. Mapping of the diffuse emission from long-lived isotopes such as ^{26}Al and ^{60}Fe and measurements of the line profiles will provide information on their sources in the galaxy.

This spectrometer can be used to measure the width and shape of the narrow 511-keV positron annihilation line from the center of our galaxy and search for similar emission from other active galaxies. Accurate measurements of cyclotron line features from Hercules X-1 and other X-ray pulsators can be obtained. Finally, it may be possible to detect γ-ray lines produced by inelastic collisions of cosmic rays with the interstellar medium.

3. INSTRUMENT PAYLOAD

The program of scientific objectives presented above determines a complement of instruments for the **MAX '91** mission. The instruments summarized in Table 3.1 are optimized for achieving the scientific objectives and were studied in some detail by the committee. The objectives and a brief description of each individual instrument are given in the following sections, with more details in the appendixes. A possible arrangement of the instruments on a platform attached to the **MMS** is shown in Figure 3.1.

In the committee discussions it was quite clear that new high-resolution imaging and spectroscopy experiments for the hard X-ray and γ-ray energy domains must share top priority. Fortunately, these experiments, although novel, have a considerable heritage of study and development. Balloon versions of high-energy imaging and spectroscopy instruments are currently being developed and are expected to be flown in the future. The Fourier-transform imaging technique has been extensively studied for the Pinhole/Occulter Facility. The Low Energy Imager (**LEI**) and the Soft X-Ray Impulsive Phase Spectrometer (**SIPS**) are based on **SMM** and rocket instruments. A number of ancillary instruments were considered by the committee and are discussed in Section 3.5.

In contrast to **SMM**, all the **MAX '91** instruments, with the possible exception of the **LEI**, have the capability of viewing the whole solar disk at one time. Consequently, no flares will be missed because of restricted fields of view. Also, the instruments can be kept pointed at, or close to, Sun center, so that spacecraft operation and control will be greatly simplified.

Table 3.1. MAX '91 Payload

Instrument	Range	Angular Resolution	Technique
Gamma-Ray Imaging Device (**GRID**)	5 keV to 1 MeV	1·5 arcsec	Fourier-transform collimators, position-sensitive proportional counters and NaI(Tl) detectors
High Resolution Gamma-Ray and Neutron Spectrometer (**HIGRANS**)	10 keV to >100 MeV	Full Sun	Cooled HPGe detectors BGO-scintillators
Low Energy Imager (**LEI**)	Soft X-rays, EUV or UV	$\sim$ 1 arcsec	Grazing-incidence and/or normal-incidence optics
Soft X-ray Impulsive Phase Spectrometer (**SIPS**)	1 to 10Å	Full Sun	Flat and bent crystals, position-sensitive proportional counters

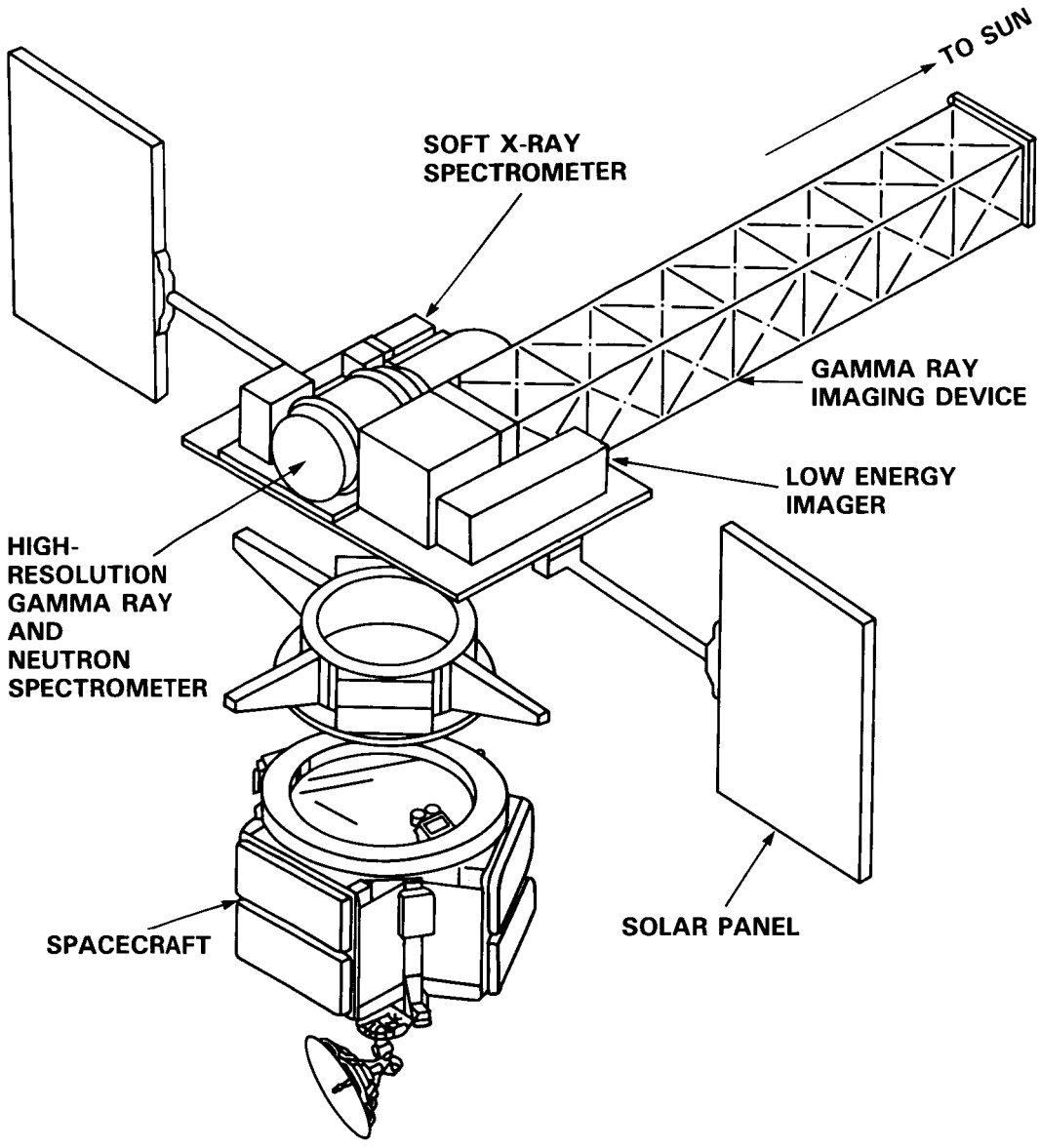

Figure 3.1. Possible arrangement of the **MAX '91** payload on a platform attached to a Multi-mission Modular Spacecraft (**MMS**). Note that the solar viewing direction is to the top right in this figure, perpendicular to the axis of symmetry of the spacecraft. This viewing direction was chosen to minimize the gravity-gradient torques resulting from the long boom of **GRID** (see Section 4.1).

3.1. Gamma Ray Imaging Device (GRID)

The primary objectives of **GRID** are as follows:

- Identification of sites of particle acceleration and interaction
- Study of the temporal and spatial development of both the thermal and non-thermal electron components of solar flares
- Imaging of the accelerated nucleon component of strong solar flares
- Hard X-ray and γ-ray imaging of cosmic sources.

Previous solar hard X-ray images have been limited to a resolution of 8 arcsec and to energies below 40 keV. A hard X-ray and γ-ray instrument such as **GRID** will have 5 to 10 times better angular resolution (1·5 arcsec), a factor of 1000 improvement in sensitivity over the **HXIS** on **SMM**, and provide a totally new capability for high-resolution imaging of solar flares at energies above 40 keV (see Table 3.2).

The greatly improved sensitivity of **GRID** will allow it to image an average of five flares per day at energies above 40 keV during the solar maximum, thus providing a large sample of high-energy flare images for statistical studies. The high sensitivity of **GRID** will also allow complete temporal imaging of moderate and strong flares on a subsecond timescale. The weak precursor hard X-ray emission expected from the corona and the low-level emission at hard X-ray and γ-ray energies from the gradual phase of the flare can also be imaged with **GRID**.

GRID is based on a Fourier-transform imaging technique, described in Appendix A1.2. Two widely spaced, fine-scale grids create a large-scale modulation pattern of high-energy photons which can be measured with a detector having only moderate spatial resolution. This modulation pattern contains the phase and amplitude information for a single Fourier component of the source distribution. Each pair of grids therefore provides information analogous to a single "baseline" in radio interferometry. Multiple grid pairs are used with a variety of slit spacings and angular orientations to sample numerous Fourier components. An image is constructed from these Fourier components in exact analogy to image formation with multi-baseline radio interferometers such as the **VLA**.

The **GRID** instrument studied by the **MAX '91** committee consists of a square array of 34 grid pairs, each with its own position-sensitive detector system. Thus, 34 separate Fourier components could be measured, corresponding to size scales in the range from 1·5 arcsec to 3 arcmin. Such sampling will produce the hard X-ray and γ-ray equivalent of the microwave image shown on the front cover of this report.

The grids are fabricated from tungsten and are placed at both ends of a 7-m-long boom the aspect of which is determined to 0·1 arcsec with an aspect sensor such as the Solar Disk Sextant (**SDS**), described in Appendix A1.3. Each detector system is made up of a multiwire proportional counter sensitive to X-rays from 5 to 50 keV followed by a NaI(T*l*) scintillation camera for higher energies up to 1 MeV.

Table 3.2. GRID instrument parameters

Technique ..... Fourier-transform imaging	X-ray detectors ..... Position-sensitive multiwire
	(5 to 50 keV) proportional chambers
Angular resolution .. 1·5 arcsec	(3 cm × 10 cm × 10 cm)
Field of view ..... Full Sun (0·6 degrees)	γ-ray detectors ..... NaI(Tl) scintillation cameras
	(50 keV to 1 MeV) (2 cm × 10 cm × 10 cm)
Boom length ..... 7 m	
	Total detector area .. 3400 cm^2
Parameters of grids	
Number of pairs ... 34	Sensitivity
Slit spacings ..... 50 μm to 6 mm	(5 to 40 keV) ..... 1000 × **HXIS**
(1·5 arcsec to 3 arcmin)	(>40 keV) ..... Totally new capability
Upper dimensions .. 17 cm × 17 cm	~5 flares per day
Lower dimensions .. 10 cm × 10 cm	
Thickness ..... 1 cm	Aspect sensors ..... **SDS** (see Appendix 1.3)
Material ..... Tungsten	

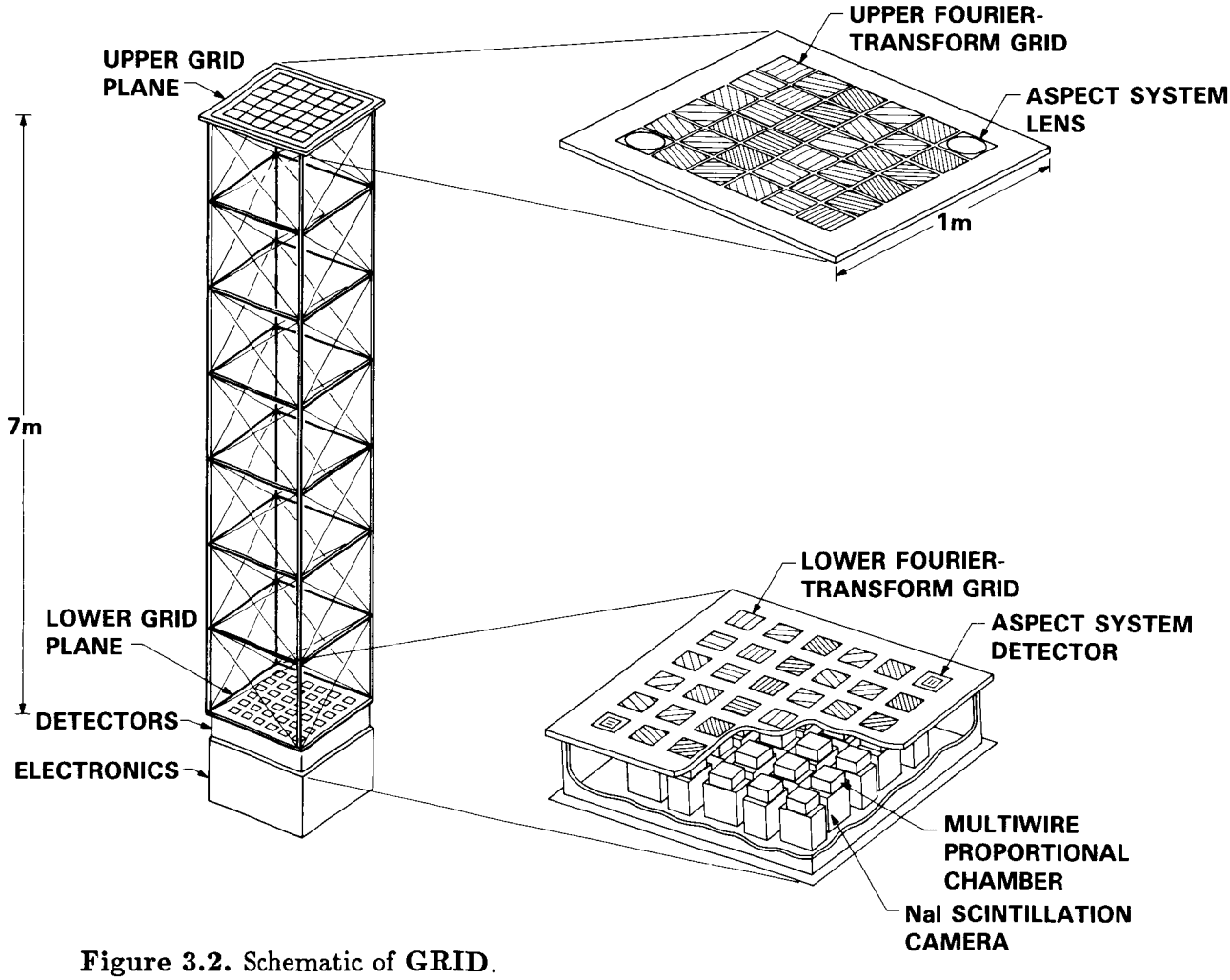

Figure 3.2. Schematic of **GRID**.

The capability of **GRID** to resolve a typical flaring magnetic loop, both spatially and temporally, is shown schematically in Figure 3.3, where the evolution of such a loop as it would appear in 20-keV X-rays is illustrated for the thermal and non-thermal models.

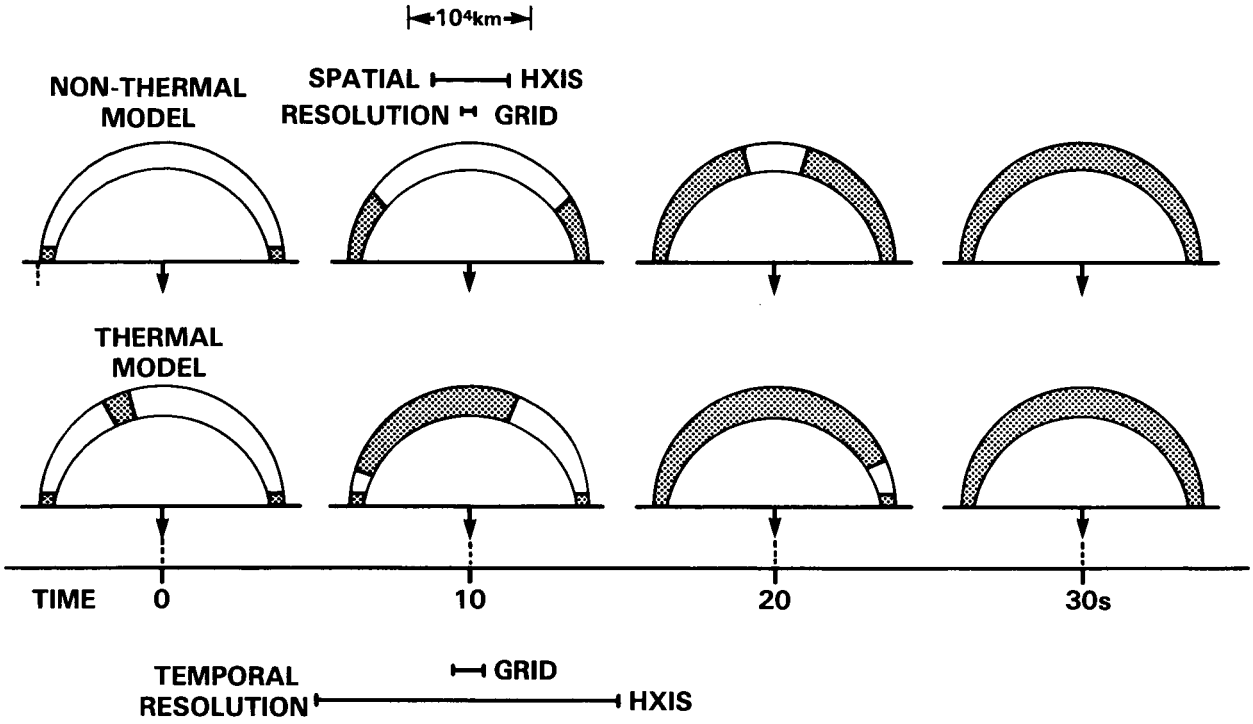

Figure 3.3. Predicted appearances of a flaring magnetic loop in hard X-rays ($\sim$ 20 keV) to show the improvements expected with **GRID**. The top and bottom row of loops show the expected evolution of the hard X-ray spatial structure in the non-thermal and thermal models, respectively. Shown above and below the figure are the spatial and temporal resolutions of **HXIS** and **GRID**.

In the non-thermal model, electron precipitation into a dense target produces the observed bremsstrahlung. As the event proceeds, the material heated by the electrons rises up the flux tube and causes the hard X-rays to be produced over a greater fraction of the loop. In the thermal model the principal source of hard X-rays is a mass of hot plasma that is situated near the loop top and grows along the loop through conductive heating of the cooler surroundings. There is also a weaker footpoint component from escaping high-energy electrons, but these electrons deposit insufficient energy to cause significant evaporation of the chromospheric target.

Figure 3.3 shows that many intermediate stages of flare evolution inaccessible to **HXIS** are observable with **GRID**. Furthermore, these images will have higher sensitivity and higher spatial resolution, and will extend to higher energies. The availability of such images will allow us to differentiate clearly between the two models, or to suggest an alternative. In this way we will be able to probe the physics of the plasma processes occurring in the loop.

3.2. High Resolution Gamma-Ray and Neutron Spectrometer (HIGRANS)

The primary objectives of **HIGRANS** are as follows:

- High-resolution observations of solar flare γ-ray lines from 300 keV to 20 MeV
- High-resolution X-ray and γ-ray continuum measurements from 10 keV to >20 MeV and moderate-resolution measurements to >100 MeV
- Flare neutron measurements from 20 MeV to 1 GeV

Measurements of the solar γ-ray line and continuum spectrum can provide unique information on the acceleration of nuclei and relativistic electrons in the Sun, including the number, energy spectrum, chemical composition, and possible beaming of the particles. Solar γ-ray spectroscopy also can determine elemental abundances in the solar atmosphere with an accuracy that could exceed that of atomic spectroscopy.

HIGRANS (shown in Figure 3.4) is designed to provide spectral resolution of a factor of about 50 higher than previous NaI(T*l*) γ-ray spectrometers. This improved resolution, shown as a function of energy in Figure 3.5, is sufficient for accurate measurement of all parameters of the expected γ-ray lines with the exception of the neutron capture deuterium line, which has an expected FWHM of about 0·1 keV.

In addition to the γ-ray line measurements, the wide energy range of **HIGRANS** permits simultaneous, sensitive, high-resolution measurements of the hard X-ray continuum from mildly relativistic electrons, the γ-ray bremsstrahlung continuum from relativistic electrons and positrons, and the γ-rays from neutral pion decay. The detection of solar flare neutrons will complement the γ-ray line measurements and supply unique data on flare protons above 100 MeV. The sensitivity of **HIGRANS** is a factor of 5 to 10 higher than that of **SMM** instrumentation for measurements of narrow γ-ray lines, hard X-ray and γ-ray continuum, and flare neutrons.

Other objectives of **HIGRANS** are as follows:

- High spectral and temporal resolution observations of cosmic γ-ray bursts
- High spectral resolution observations of cosmic γ-ray and hard X-ray discrete and diffuse sources

The instrument consists of an array of high-purity, n-type, coaxial germanium detectors (HPGe) cooled to 90 K and surrounded by bismuth germanate (BGO) and plastic scintillator anticoincidence shields. Each HPGe detector is electrically divided into a thin front segment and a thick rear segment to give optimal signal/background for photons over the energy range 10 keV to 20 MeV. Neutrons and high-energy ($\geq$20 MeV) γ-rays are detected and identified with the combination of the HPGe detectors and rear BGO shields. Table 3.3 gives the parameters of **HIGRANS**; further details are given in Appendix 2.

Table 3.3. HIGRANS instrument parameters

Energy range	
γ-rays and hard X-rays	10 keV to 20 MeV (high-resolution HPGe) 20 MeV to >100 MeV (medium resolution BGO)
Neutrons	20 MeV to 1 GeV
Energy resolution	0·6 to 5 keV FWHM (high-resolution HPGe) (see Figure 3.5)
Total detector area	340 cm^2 HPGe 1400 cm^2 BGO
Field of view	60° FWHM
Shields	5-cm-thick BGO on sides, three 5-cm thick BGO at rear, 1-cm-thick plastic scintillator over 4π steradians
Germanium detector cooling	90 K for 3 years with solid-cryogen cooler

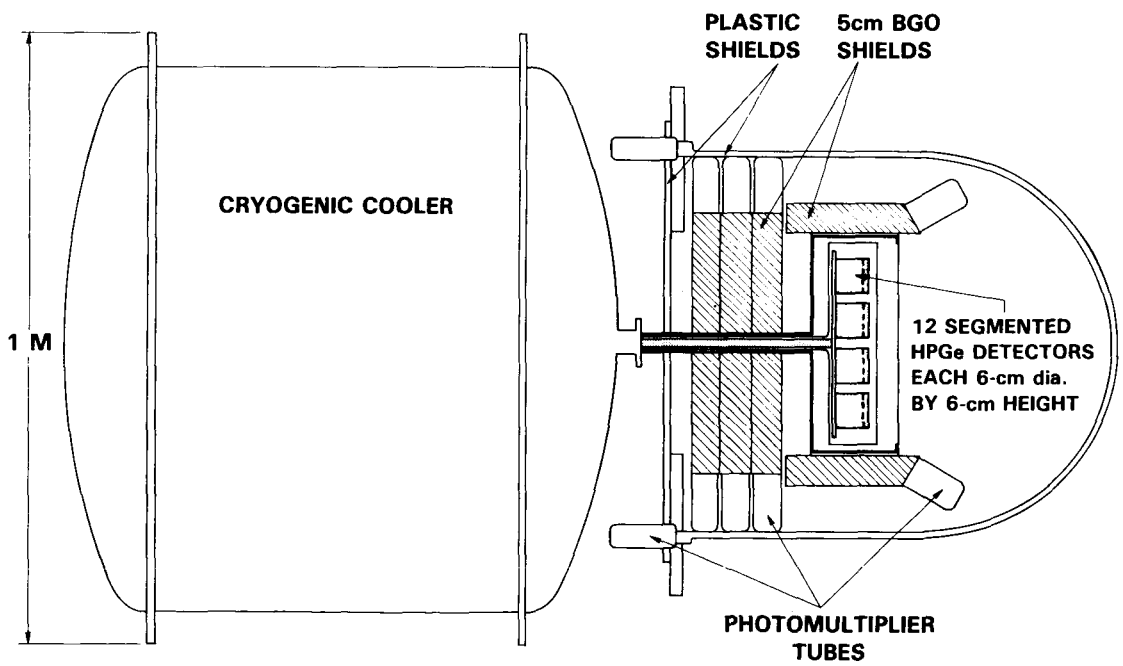

Figure 3.4. Schematic of **HIGRANS**.

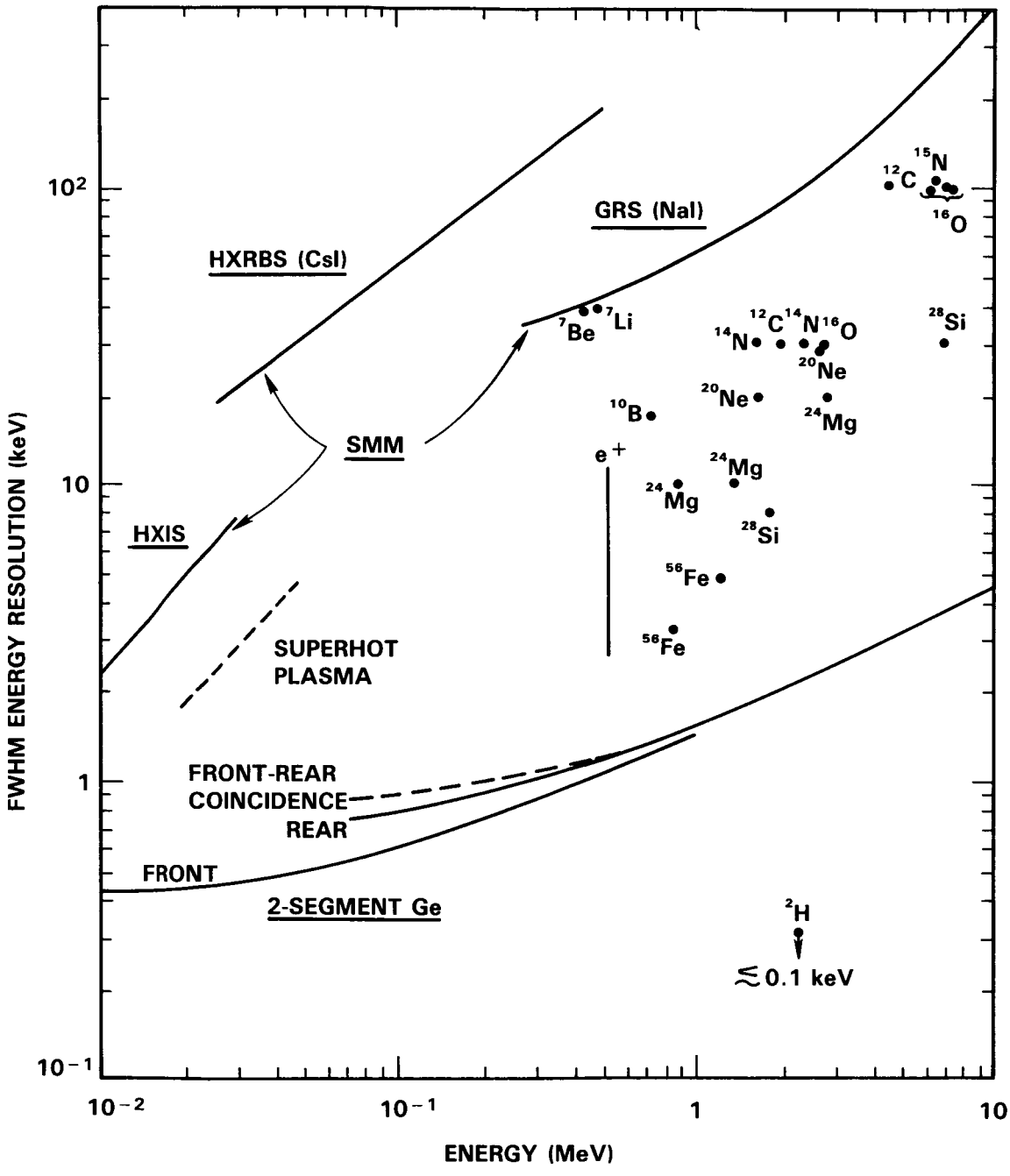

Figure 3.5. FWHM energy resolution of the hard X-ray and γ-ray detectors on SMM plotted as a function of the photon energy for comparison with the resolution of the HIGRANS cooled HPGe detectors. Also shown are the predicted widths of the γ-ray lines expected in solar flares and the resolution required to resolve the extremely steep spectrum of the superhot plasma.

3.3. Low Energy Imager (LEI)

To relate the high-energy results to the preflare conditions and to the lower-energy thermal flare, it is necessary to have images of the flaring plasma at high temporal and spatial resolution for electron temperatures between about 10^5 and 20×10^6 K. Subsecond temporal resolution is required to detect the rapid variations that occur during the impulsive phase, particularly in the transition zone lines. Images at lower transition region temperatures ($\approx 10^5$ K) reveal that the chromospheric plasma is heated either by electron beams or by thermal conduction from the overlying hot coronal plasma. Images at temperatures greater than a few million degrees reveal the morphology, energetics, and evolution of the soft X-ray coronal flare. Plasma parameters such as electron density, differential emission measure and filling factor, and the characteristics of plasma motions, can be determined from such images.

Knowledge of the shapes, sizes, and orientations of flare loop systems and the plasma properties in flare footpoints is necessary for understanding energy release processes. From the observed source sizes and their filling factors, for example, we can infer the scale size of the interaction region in which the observed lines are formed. Images over a broad temperature range will enable the release and transport of flare energy throughout affected regions of the solar atmosphere to be determined. A long-standing issue revolves around the relationship of the coronal thermal plasma to the source or sources of hard X-ray emission. Thus, the inclusion of an **LEI** with about 1-arcsec spatial resolution is essential for achieving the scientific goals of **MAX '91**.

In the time available, the Working Group was unable to judge which specific instrument would be best suited for **MAX '91**. Rather than assign priorities to the candidate instruments, the Working Group encourages proposals of instruments, with the final choice for the **LEI** made by evaluating the actual proposals. The Working Group did decide, however, that cost considerations mandate that only one **LEI** be selected for the primary payload.

An **LEI** could operate in the UV (1100 to 3200 Å), the EUV (100 to 600 Å), or the soft X-ray (< 100 Å) wavelength region. All three of these wavelength regions contain emission lines that would provide valuable diagnostic information for the scientific objectives. For the images to be useful, each image should be confined to a single spectral line so that it represents a well-defined range of temperatures. Two or three lines per decade of temperature range provide adequate temperature coverage, since any given ion is typically abundant over a range of about 0·3 in the log of the temperature. The spectrum above 1100 Å is complex and requires a spectograph to isolate lines except for Lyman-α, which can be observed with a filter, and C IV, for which a Fabry-Perot interferometer can be made. The spectrum between 200 and 600 Å is also complex, requiring a spectrograph. Between 100 and 200 Å, it may be possible to isolate a few lines with multilayer mirror technology, in which a normal-incidence mirror blank is coated with alternating layers of materials with widely differing atomic number to produce Bragg reflection at a specified wavelength. There are a number of well separated lines between 44 and 100 Å that can be isolated with multilayer mirrors.

Information on a wide variety of temperature domains and physical processes is available in the UV wavelength region. Allowed and intersystem lines formed in the lower transition region at about 10^5 K have been shown with **UVSP** to be sensitive indicators of the deposition of energy in the chromosphere. These UV lines are formed at temperatures ranging from photospheric to about 2×10^5 K. From their temporal coincidence with impulsive high-energy

emissions, they are interpreted to be the result of bombardment by energetic flare particles such as electron beams. In addition, the UV region contains several forbidden lines from coronal ions formed at temperatures of about 10^6 K, as well as the 10^7 K Fe XXI line at 1354 Å, thus providing some information on high-temperature plasma. The presence or absence of low-energy proton beams (<1 MeV) might be inferred from spectral signatures that are predicted to occur in the red wing of Lyman-α. Considerable information can be obtained on velocity fields and electron densities from line profiles and line ratios.

The EUV wavelength region contains a wealth of emission lines, spanning a temperature range from about 5×10^4 K (He II) up to about 20×10^6 K (Fe XXIV). Images in the EUV could provide a more complete temperature coverage than is possible in the UV, particularly because the UV forbidden lines (except Fe XXI) are rather weak. Other advantages of imaging in the EUV compared with the UV include extension to a significantly higher temperature, information on plasma motions from line profiles, and many density-sensitive line ratios. The lower-transition-region lines that brighten simultaneously with hard X-ray bursts and that indicate energy deposition in the chromosphere are best observed in the UV, however, and the test for low-energy proton beams cannot be done in the EUV.

The soft X-ray region provides diagnostics for plasma temperatures in excess of about 4×10^5 K. In particular, the He-like lines of C V and O VII may allow the study of chromospheric heating by electron beams, and the superhot component of flares at temperatures of about 35×10^6 K can be observed in spectral lines of Fe XXVI. An attractive feature of the soft X-ray region is that a conventional X-ray telescope can provide full-Sun images at high spatial resolution, thereby eliminating the need for a flare flag and instrumental mechanisms for acquiring the flare region.

The Working Group discussions centered on low-cost approaches to the instrumentation for an **LEI**. Three of the approaches would reuse existing hardware to save cost, while two others are based on multilayer mirror technology. All approaches were based on the use of charge-coupled device (CCD) arrays or other imaging detectors. The options considered included the following:

1. Refurbish and upgrade **UVSP** when the **SMM** is recovered from orbit. This system is a grating spectrograph and operates in the spectral range from 1200 to 3000 Å. The **UVSP** optomechanical system would be reused, with the original detectors replaced by a CCD array and with the addition of a telescope of longer focal length and larger aperture (see Appendix 3.1).

2. Adapt an existing flight-spare grazing-incidence telescope from the **Skylab** program. By addition of array detectors and a filter system based on thin metallic films and/or multilayer tertiary mirrors, a filtergraph system could be made to operate in the spectral range from 1 to 200 Å, with single lines isolated between 44 and 200 Å (see Appendix 3.1).

3. Complete the development of a grazing-incidence EUV telescope and normal-incidence grating spectrograph system that was partially developed under the **Spacelab** program. This instrument, called the Solar Extreme Ultraviolet Telescope and Spectrograph (**SEUTS**), uses CCD arrays and covers the spectral range from 220 to 470 Å. It will produce images similar to those of the **NRL-Skylab** spectroheliograph but with the advantage that the images would not overlap (see Appendix 3.3).

4. Prepare an X-ray/EUV normal-incidence imaging instrument, with multilayer prime-focus mirrors to both form the images and define the passbands. A proof-of-concept instrument of this type has been successfully flown on a sounding rocket. The version discussed with the working group used four mirrors feeding a single detector to sample four different spectral lines. It is a filtergraph system and operates in the wavelength range from 44 to 200 Å (see Appendix 3.2.).

The filtergraph options have the advantage that they view the whole Sun simultaneously but suffer from a lack of spectral resolution. Their wide fields of view make them excellent candidates for the flare-finding function and for the determination of the overall morphology. The spectrographs, on the other hand, have good spectral resolution when used with a slit at the image plane, but only observe points along a chord of the solar disk, rather than simultaneously observing the entire Sun. When used with a CCD detector, a spectrograph can observe a square field equal in size to the projected slit length in one CCD frame time (assuming a square CCD format). These fields were 5 and 8 arcmin, respectively, for options 1 and 3. It is possible to operate a spectrograph in a slitless mode, as discussed in Appendix 3, but the field size/rate limitation still applies, since this limit is set by the rate at which pixels can be read out by the CCD electronics. One solution may be to prepare a filtergraph and spectrograph combination (see Appendix 3.1).

3.4. The Soft X-Ray Impulsive Phase Spectrometer (SIPS)

The **SIPS** instrument (shown in Figure 3.6 and described in detail in Appendix 4) consists of eight high-sensitivity bent-crystal spectrometers (**HSBCS**) and two high-sensitivity flat-crystal spectrometers (**HSFCS**). The wavelength coverage is given in Table 3.4.

SIPS will provide, for the first time, soft X-ray spectra on a timescale characteristic of the impulsive phase ($\leq$ 1 s). This is accomplished by an improvement in sensitivity of at least a factor of 10 over the equivalent instruments on **P78-1** and **SMM**. Hence, **SIPS** will provide measurements of plasma temperature, density, emission measure, and motions from the onset of the impulsive phase (earlier than before) and with sufficient sensitivity to detect variations on timescales of $\leq$1 s. This instrumentation makes possible the following new investigations:

- **Measurements of transient ionization. SIPS** will have sufficient sensitivity to search for transient ionization effects in X-ray spectra obtained during the impulsive phase. Such observations will provide, for the first time, estimates of the density of the high-temperature plasma during the impulsive phase that are independent of the filling factor.
- **High-temperature differential emission measure.** The flare plasma is known to be multi-thermal. **SIPS** will observe at least five different lines representing temperatures between 3×10^6 and 50×10^6 K with a temporal resolution of 1 s. This vastly improved capability will allow the temperature distribution of the plasma during the impulsive phase to be measured and thus enable the primary heating function to be determined.
- **Coronal abundances. BCS** has determined the coronal abundance of Ca and obtained evidence to suggest that it varies for different flares. **SIPS** will be capable of determining the abundances of many more elements (Mg, Al, Si, S, Ar, K, Ca, Ti, Mn, Cr, Fe, and Ni) with higher accuracy than previously possible. Additionally, the **SIPS** and **HIGRANS** measurements will provide a unique opportunity to study abundances simultaneously at different heights in the solar atmosphere.
- **Plasma upflows and turbulent motions.** Pioneering observations of plasma upflows and turbulent motions were made with **SMM**, **P78-1**, and **Hinotori**. **SIPS** will observe these phenomena with higher time resolution and earlier in the impulsive phase. Furthermore, **SIPS** will provide the first measurement of the flare plasma dynamics as a function of temperature. Another exciting possibility is the combination of these velocity measurements with the 1-arcsec images of the flare loops obtained with **GRID** and **LEI**.
- **Superhot component.** The superhot component will be observed in the high- temperature lines of Fe XXVI and Ni XXVII. The spectroscopic observations will complement those made with **HIGRANS** by allowing the determination of the electron temperature, emission measure, and indications of departure from thermal equilibrium. This provides electron density and evidence for the presence of non-Maxwellian electron distributions.

In summary, **SIPS** will provide improved measurements of plasma parameters with higher time resolution and earlier in the flare than previously possible. The knowledge of these plasma parameters is crucial for an understanding of the plasma dynamics and the flare energetics during the impulsive phase and into the gradual phase. The instrument design relies on proven technology, yet represents an enormous improvement over previously flown soft X-ray spectrometers. It should yield a wealth of new science in its own right and will support the goals of the other **MAX '91** instruments.

Table 3.4. Principal characteristics of SIPS

Instrument	Channel	Wavelength Coverage (Å)	Number of Detectors	Spectral Resolution ($\lambda/\delta\lambda$)
HSBCS	Ca XVIII–XIX	3·160 – 3·235	3	5000
	Fe XXII–XXV	1·840 – 1·985	3	12500
	Fe XXVI	1·769 – 1·796	2	5000
HSFCS	Low Temp.	1·0 – 9·5	1	15000
	High Temp.	1·0 – 4·0	1	15000

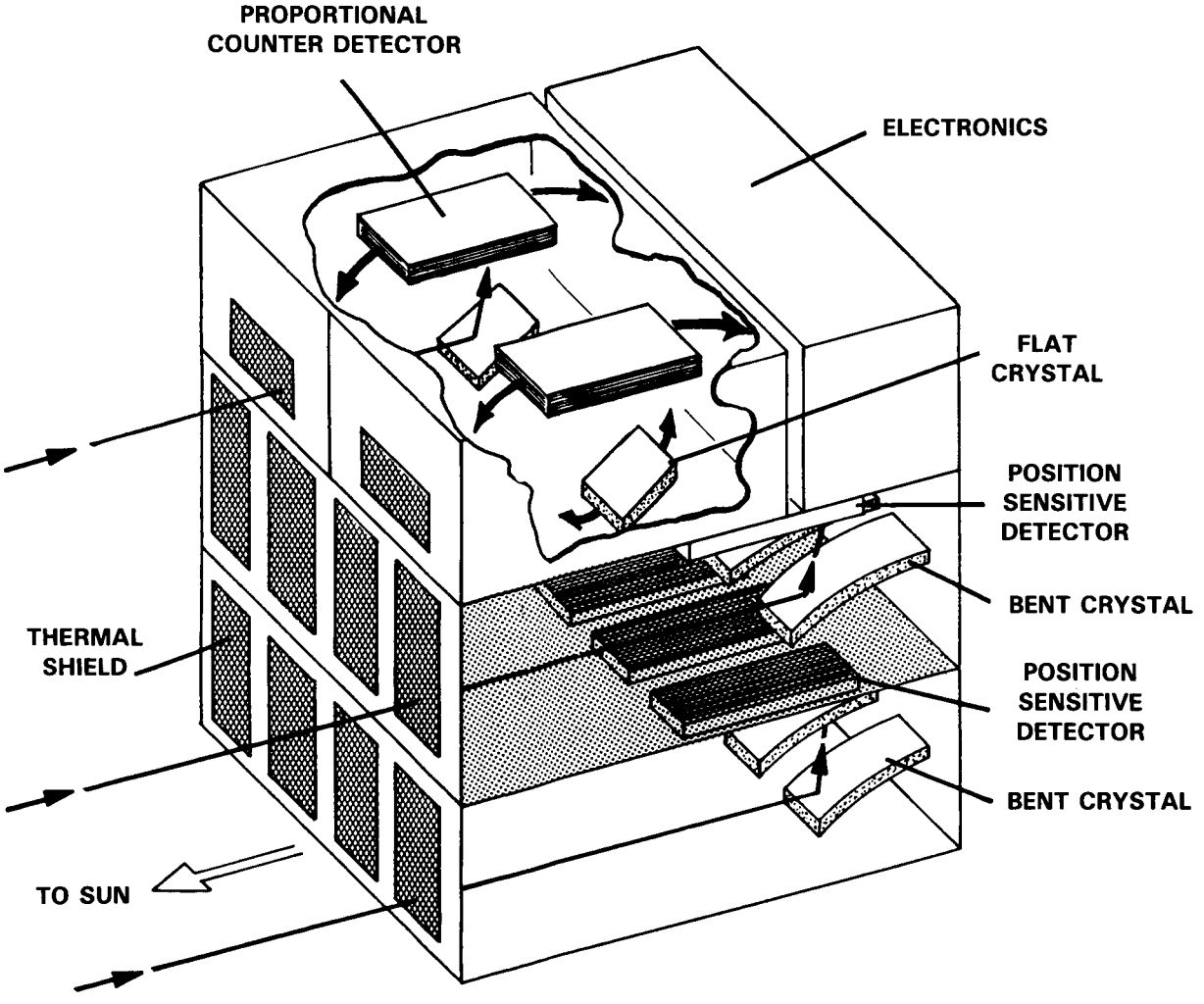

Figure 3.6. Schematic of SIPS.

3.5. Additional Instrument Candidates

The four instruments described in the preceding sections constitute an integrated payload for the study of high-energy solar physics. The **MAX '91** Science Working Group believes that this basic payload should be given highest priority for the next solar maximum. Several additional instrument candidates were studied by the Committee, and, although they have not been suggested as primary instruments, their inclusion on an augmented **MAX '91** payload or on other carriers is highly desirable. In general, these additional instruments provide observations that are complementary to those of the four primary instruments. Three of the additional instruments studied by the Committee are discussed below, and a possible scenario for future augmentation of the basic **MAX '91** payload is outlined.

▪ Active Cavity Radiometer Irradiance Monitor II (ACRIM II)

This instrument is designed to extend the **SMM-ACRIM** observations of total solar irradiance into Cycle 22. **ACRIM** is a very precise radiometer, capable of parts-per-million precision; the time series of data obtained since 1980 shows variations on all timescales up to its sampling limit of 3·8 mHz. For maximum possible continuity of the **ACRIM** data set, it would be desirable to include **ACRIM II** in the initial **MAX '91** payload.

The observed variations of the total solar irradiance include components due to sunspots and faculae with timescales of days to weeks, granulation in the photosphere with timescales of minutes to days, and solar global oscillations (low degree p-modes). Extended observations of these variations, and of others as yet unidentified, will substantially add to our knowledge of the solar interior. It may be possible through such data to obtain empirical information on the nature of convection in stellar envelopes and on the origin of stellar magnetism. On the longest timescales, the observation of secular or solar cycle variations would obviously have profound importance for our understanding of the influence of the Sun on the climate of the Earth.

▪ Solar Disk Sextant (SDS)

The **SDS** is an instrument designed for accurate measurements of solar size, shape, and variations. It would consist of a beam-splitting wedge which casts a series of solar images onto an array of linear detectors. **SDS** is especially attractive in the context of the **MAX '91** payload, because it can fulfill the dual role of a basic science instrument and an aspect-sensing system for **GRID**. The concept studied by the Committee would involve integrating **SDS** into the **GRID** instrument to provide high-accuracy measurement of the relative orientation of the two grid planes with respect to Sun center (see Appendix 1.3).

By precisely measuring the size and shape of the Sun and their variation with time, **SDS** addresses questions relating to the physics of the solar interior. Variations in the solar size should be directly correlated with variations in the solar energy output. Combined with data from an **ACRIM** instrument, the **SDS** measurements will provide important clues to the physical origin of these variations and thus contribute to our basic understanding of solar luminosity. Measurements of the solar shape will provide accurate data on solar oblateness and quadrupole moment. These data bear directly on theories of solar evolution and interior dynamics, and on tests of gravitational theories. Additionally, variations in the solar shape reflect pulsations of the Sun, a phenomenon of extreme current interest to the field of helioseismology. **SDS** should be particularly effective for studying pulsations in the long-period regime, in which standard Doppler techniques are least sensitive.

▪ High-Energy X-Ray Polarimeter (HXP)

An X-ray polarimeter operating between 10 and 100 keV would be extremely valuable for solar flare observations. The two major categories of flare models, thermal and nonthermal, differ significantly in their polarization signatures: the thermal models predict polarizations of at most a few percent, while electron beam models predict strongly polarized emission, especially in coronal parts of the flare loop. Polarimetry measurements are particularly powerful because they can provide direct evidence of the degree of anisotropy from observations of a single flare without necessitating statistical studies of a large number of independent events or multispacecraft stereoscopic observations.

HXP would detect polarization by utilizing the asymmetry of Compton scattering of polarized incident photons. The polarimeter consists of 37 active scintillator scattering targets surrounded by an array of 132 NaI(T*l*) detectors. This arrangement achieves a 1σ sensitivity of 1·1 % polarization at 30 keV in 10 s from an M2 flare.

▪ MAX '91 Payload Augmentation

It was recognized by the Committee that changes to the **MAX '91** core payload might be valuable over time. In particular, after the decline of solar flare activity expected by 1996, a transition to quiet-Sun observations might be desirable. The addition of new instrumentation, for instance a visible/UV coronograph or an upgraded, high-resolution soft X-ray telescope, will be advantageous at that time.

The concept of in-orbit payload augmentation calls for periodic visits to the spacecraft for replacement or addition of payload modules and replenishment of consumables. The design of the initial **MAX '91** payload should take this possibility into account.

3.6. Supporting Activities

▪ Other Spacecraft

The Japanese High Energy Solar Physics (**HESP**) mission, planned for launch into low Earth orbit in the early 1990's, has similar objectives to those of the **MAX '91** program. The primary instruments are a hard X-ray imaging instrument and a soft X-ray telescope but the payload will also include a γ-ray and neutron spectrometer, a Bragg crystal spectrometer, and two X-ray continuum spectrometers. Since the total **HESP** payload must be less than 120 kg, compared with over 1500 kg for **MAX '91**, these instruments lack many of the critical capabilites of the **MAX '91** instruments, in particular the high spatial resolution of **GRID** (**HESP** has 5 arcsecond resolution, and that only up to 70 keV), the high energy resolution of **HIGRANS**, and the high sensitivity of **SIPS**. Nevertheless, **HESP** would provide valuable supporting observations for the **MAX '91** mission.

GRO also will provide spectral measurements of solar and cosmic X-ray and gamma-ray sources. This 15000-kg spacecraft features several high-sensitivity NaI(T*l*) spectrometers, a spark chamber, and a Compton telescope. X-ray and gamma-ray spectra will be obtained over the energy range from 30 keV to hundreds of MeV and neutron spectra from 20 MeV to 500 MeV. None of the instruments, however, has any imaging capability for solar flares, and they lack the high-energy resolution of **HIGRANS**.

Direct measurements of the energetic particles which are accelerated in flares and escape to the interplanetary medium will be invaluable in support of the **MAX '91** hard X-ray and

γ-ray observations. The flux, energy spectrum, elemental and isotopic composition, and ionization state of the accelerated particles can be determined with instruments on spacecraft outside the Earth's magnetosphere. In the latter part of the next solar maximum (1991–1995), such energetic-particle measurements are planned for the International Solar Terrestrial Physics (**ISTP**) program, on the Japanese **GEOTAIL** spacecraft, the European Solar and Heliospheric Observatory (**SOHO**), and the U.S. **WIND** spacecraft. In addition, the **Ulysses** spacecraft (International Solar Polar Mission) will be in heliocentric orbit over the poles of the Sun. This spacecraft will provide hard X-ray observations as well as measurements of energetic particles. Of particular interest here is the possibility for stereoscopic measurements of solar hard X-ray bursts with **MAX '91** and **Ulysses** to provide information on the height structure and directivity of the hard X-ray source.

The **SOHO** instruments include a white-light and Lyman-α coronagraph and a grazing-incidence EUV spectrometer. These instruments could supply very important supporting and complementary observations for the **LEI**. The coronagraph in particular will extend the **MAX '91** observations from the inner corona and chromosphere out into the interplanetary medium. It is now known that coronal mass ejections (CMEs) observed with coronagraphs tend to be associated with long-duration flares when they are associated with flares at all. These flares last for many hours, in contrast to events that last 1 h or less. Why long-duration events should preferentially be associated with CMEs is a major unanswered question about solar activity. The **MAX '91** experiments could make important contributions to answering this question.

- **Ground-Based Support**

To fully exploit the potential of hard X-ray and γ-ray imaging and spectroscopy and to achieve the scientific objectives outlined in Section 2, a coordinated program of ground-based observations is required. Optical observations such as Hα, while representing the lower-energy, thermal aspects of the flare, indicate the morphological framework within which the high-energy imaging data must be interpreted. Ground-based magnetographs are essential to provide the basis for understanding the magnetic field configuration from which the flare energy is derived and which guides the accelerated particles.

Radio observations are required over a broad wavelength range to complement the X-ray and γ-ray observations. These include imaging and spectroscopy at metric and decimetric wavelengths and in microwaves and millimeter waves with angular and temporal resolutions commensurate with the high-energy observations.

Radio emission also is prompt, and its observation provides a complementary picture of the high-energy processes. At meter and decimeter wavelengths, coherent plasma processes generate readily detectable emission from electrons on open field lines as well as from the electrons in the closed loops which dominate the X-ray emission. At centimeter wavelengths, the preflare emission can be used to measure the magnetic fields in the low corona where the energy release is thought to occur; the impulsive phase emission gives information on electrons with energies above about 100 keV. The combination of microwave and X-ray imaging is especially powerful since the radio emission is weighted by the magnetic field strength and the X-ray emission is weighted by the ambient density.

To achieve the required complementary observations, ground-based observers can draw upon the significant, ongoing improvements in both scalar and vector magnetograph capabil-

ity, the use of video technology to provide optical data with improved time resolution, and more effective techniques for the determination of absolute coordinates of solar features for co-location of X-ray, radio, and other images. Corresponding recent developments in imaging at radio wavelengths include improved foreign facilities for imaging at meter wavelengths; an upgraded **VLA** time resolution of 3·3 s as well as its extension to longer decimeter wavelengths; a facility for performing spatially-resolved microwave spectroscopy; and the possible extension of spatially-resolved observations to millimeter wavelengths by using both U.S. and Japanese facilities.

4. TECHNICAL APPROACH

4.1. General Considerations

The approach taken in this study was to look at the reuse of an already existing MMS for the MAX '91 payload. Several MMSs may be available in the time frame of interest, including SMM and LANDSAT 4.

In our deliberations with the science community as well as the program offices at NASA Headquarters, the concept of reusing NASA's orbiting capital assets became very intriguing. The fact that the concept couples the use of an existing orbital platform, SMM or LANDSAT 4, with a new science payload brings about new programmatic economies and allows more science to be accomplished over a given period than was possible before the operational era of the Space Shuttle. The reuse of an available MMS-type observatory not only allows for a significant spacecraft budget savings, but also allows a considerable savings to be made in the cost of the flight software, the payload operations, the control center, and the experiment operations facility. In an absolute sense, the MAX '91 mission with an existing MMS becomes an extension of the SMM capability at minimum additional cost.

The mission plan calls for the new instrument module assembly to be designed in such a way that, on subsequent visits, new and more challenging instruments could be taken up to either replace or be added to the initial MAX '91 complement. The MAX '91 payload and any subsequent instruments will all be modular in design, at least at the instrument system level. Complicated instruments with consumables, such as the cryogen for the HIGRANS cooler, could be designed for subsystem modularity and for resupply in orbit.

This type of instrument packaging will facilitate a significant degree of pioneering. A principal investigator (PI) at a university or research center would now be able to design an instrument without having to become expert in spacecraft design and operations. Spacecraft interface hardware and specifications would be provided to individual PIs, who would proceed to build and test their instruments to those interfaces. Furthermore, since each instrument is fully self-contained in its own structural module, it may be possible in many cases to carry the individual instruments to orbit in load-isolation canisters, thus significantly reducing the environmental design requirements of an instrument.

Through individual instrument modularization, reduction of interface complexity, and environmental design criteria, individual universities and research institutions will now have the opportunity to apply PI-type "tender loving care" in the development of new low-cost science instrumentation.

One of the most successful aspects of SMM was the Experiment Operations Facility (EOF). In this facility, each instrument team used its own computer for instrument control and data analysis. The communication among the scientific teams that resulted from the proximity of these computers to the spacecraft control center and to each other enabled both closely coordinated observing sequences and extensive collaborative data analysis to be carried out. Such collaborations are particularly important for solar flare studies for which emissions from across the electromagnetic spectrum must be simultaneously compared. MAX '91 will continue and expand such a facility by exploiting new technologies such as computer networking. The convenient exchange of data, images, and text that can be anticipated will add new dimensions to the involvement of guest investigators.

4.2. Compatibility with the MMS

The technical approach is presented in this section for the assembly of the **MAX '91** payload into an instrument module and its integration with an **MMS**. The weight, volume, power, and telemetry requirements of the four strawman instruments are given in Table 4.1. The capability of each of the **MMS** subsystems is compared with these requirements, and the additional hardware and software required to achieve an operational spacecraft are assessed.

Table 4.1. Physical characteristics of the **MAX '91** instruments

Instrument	Volume (m^3)	Weight (kg)	Power (watts)	Telemetry(kbps) Peak	Average
GRID	1·3 × 1·3 × 1·5 (plus 7-m boom)	500	200	250	20
HIGRANS	1·3 × 1·3 × 1·3	800	200	1000	10
LEI	0·4 × 0·4 × 2·0	115	50	1000	10
SIPS	0·3 × 0·9 × 0·8	150	45	40	40

The **MAX '91** instrument module, unlike that of **SMM**, will be truly modular. Not only will the whole instrument complement be designed to be easily removed from the spacecraft, but each instrument will be mounted to facilitate accessibility and changeout. Furthermore, the instrument module will be designed to accommodate future additional instruments.

The **MAX '91** mission structure will consist primarily of the mission adapter and instrument plate assembly – the structural interface between the instruments and the spacecraft (Figure 3.1). The mission adapter will have provisions for accessible mounting of additional spacecraft electronics such as tape recorders, a power switching unit, remote interface units (RIU), and a multichannel data formatter. One concept for the mission adapter is a 24-inch-high aluminum cylinder which connects the **MMS** transition adapter ring to the instrument plate with struts to provide structural stiffness.

The instrument-mounting plate will act as the **MAX '91** optical bench. Each instrument and its associated electronics will be mounted on the plate as a complete assembly. Standard **MMS** modular fasteners and blind-mate electrical connections will be used to provide a kinematic mount that will facilitate integration and deintegration.

The most important aspect of the **MAX '91** payload that must be considered in integrating it on an **MMS** is that of the gravity-gradient torques and the capability of the **MMS** reaction wheels to overcome them. Thus, it is particularly important to orient **GRID** with its 7-m boom so that the spacecraft moments of inertia about the three principal axes do not differ from one another by more than 1200 slug ft^2, the limiting difference that the standard **MMS** reaction wheels can accommodate. This is achieved by mounting the boom perpendicular to the **MMS** axis of symmetry, as shown in Figure 3.1. The other instruments are then pointed in the same direction, with their locations on the mounting plate determined by the satellite mass properties, the instrument dimensions, and their fields of view.

The different pointing direction and mass properties of the **MAX '91** payload compared with that of **SMM** will have little effect on the attitude control system. The differences can easily be handled by new attitude control software for the onboard computer. Furthermore, the **MAX '91** pointing requirements – 2-arcminute placement and 2-arcsecond-per-minute stability – are considerably less stringent than those for **SMM** and are well within the capabilities of the standard **MMS** attitude control system. In fact, less expensive fine Sun sensors than those on **SMM** could be used to achieve the rather modest 2 arcmin placement requirement. Satisfying the stability requirement follows easily from the benign **MMS** environment, in which the only moving parts are the reaction wheels. The most difficult requirement is the determination of **GRID** and **LEI** pointing to 0.1 arcsec; this will be achieved by using **SDS**, as discussed in Appendix 1.3.

The same command and data handling scheme used on **SMM** will accommodate the **MAX '91** payload, with the exception that the onboard tape recorders will be augmented with two 10^9-bit recorders to handle the large data requirements of the different instruments. As with **SMM**, each instrument will have one or more standard RIUs. The telemetry system will be similar to that used on **SMM**, with the exception that the real time data rate will be increased to 64 kbps and both tape recorders will be dumped each orbit via **TDRSS**.

The total power requirements of the strawman **MAX '91** payload are 1500 watts peak and 700 watts steady load. The standard **SMM** solar arrays can supply a steady 800 watts. Thus, a new 165-ft^2 set of solar arrays is required. A new set of batteries and a new power switching unit will also be required. The solar arrays will be attached to both sides of the mission adapter. No articulation is required, since the instruments will spend most of the time pointing at the Sun. As with **SMM**, offset pointing can be carried out at night or, for limited periods, during the satellite day.

One difference from **SMM** arises because of the different orientation of the **MMS** with respect to the Sun. This will produce a different thermal environment, but it can easily be handled if the **MMS** power module is kept on the side facing away from the Sun.

5. CONCLUSIONS

The program described above represents a scientific and technical response to the major discoveries made with **SMM** and other observatories during solar cycle 21. The recovery and multiple reuse of an existing **MMS** appears to offer us a chance to meet the schedule of the solar cycle with innovative new instruments, centering on the hard X-ray and γ-ray astrophysics that allows us to study non-thermal particles. These observations will give us the first opportunity to explore the interactions of these particles in the flaring plasma.

The two high-energy instruments in the **MAX '91** payload are both novel; they accomplish arcsecond imaging and high-resolution spectroscopy of hard X-rays and γ-rays. In both cases there is an excellent technical heritage: **GRID** was developed from the concept of the Pinhole/Occulter Facility that has been studied extensively for flights on the Shuttle and Space Station; **HIGRANS** is derived from several balloon payloads with HPGe detectors.

These major experiments will be incorporated with a set of supporting instruments to make a coordinated set of data available for observatory-type use. The value of the observations will be further enhanced by simultaneous ground-based radio, microwave, and optical observations. The **MAX '91** Committee believes that the suggested payload will return a wealth of new scientific results that will advance our understanding of solar flares in particular and high-energy plasma physics in general.

APPENDIX 1. GAMMA RAY IMAGING DEVICE (GRID)

A1.1. Instrument Description

The **GRID** instrument studied by the Committee is shown in Figure 3.2 and consists of the following components:

- 34 pairs of Fourier-transform grids
- 34 modular X-ray detectors
- 34 modular NaI(T*l*) γ-ray detectors
- two **SDS**s for precise aspect information

The two planes of Fourier-transform grids are placed at the ends of the 7-m boom. The slit widths increase logarithmically from 50 μm to 0·6 cm, corresponding to angular resolutions of 1·5 arcseconds and 3 arcminutes, respectively. Angular orientations are chosen to give uniform sampling of the u-v plane of spatial frequencies. An important technical simplification of Fourier-transform imaging is that the alignment of the grids need not be maintained to the arcsecond precision implied by the resolution. Post facto knowledge (as distinct from real-time control) of the alignment is adequate in this respect. The nominal thickness of the grids to provide sufficient attenuation for γ-rays up to 1 MeV is 1 cm of tungsten.

The X-ray detector system consists of 34 modular one-dimensional xenon multiwire proportional chambers. Similar but larger chambers have been developed for use on a **Spacelab** experiment. These will cover the energy range from 5 to 30 keV with good sensitivity and will give moderate sensitivity up to 60 keV, providing overlap and intercalibration with the γ-ray detector system.

The γ-ray detector system will consist of 34 modular NaI(T*l*) scintillation cameras with one-dimensional position resolution. The technology for NaI scintillation cameras has been developed and employed extensively for a variety of γ-ray observations including medical applications and balloon-borne instruments. The nominal thickness of the NaI detectors is 2 cm, giving good conversion efficiency up to 1 MeV. The position resolution of the detectors will be better than 1.5 cm over the entire energy range; the FWHM energy resolution will be 12% at 100 keV and 7% at 1 MeV.

A1.2. Fourier-Transform Imaging

The operating principle of **GRID** is based on the concept of Fourier-transform imaging. Figure A.1 provides a schematic illustration of the technique. Each collimator grid consists of parallel slits with a specific orientation and slit spacing. The characteristic large-scale modulation pattern at the detector plane arises from a small, controlled, difference in slit spacing between the top and bottom grids. Each pair of collimator grids allows the measurement of the phase and amplitude of a particular Fourier component of the source angular distribution. In analogy to radio astronomy, each pair of collimators provides one baseline for measurement of the angular source distribution. The phase and amplitude information from the individual γ-ray measurements is then combined to form images by using algorithms identical to those of radio astronomy.

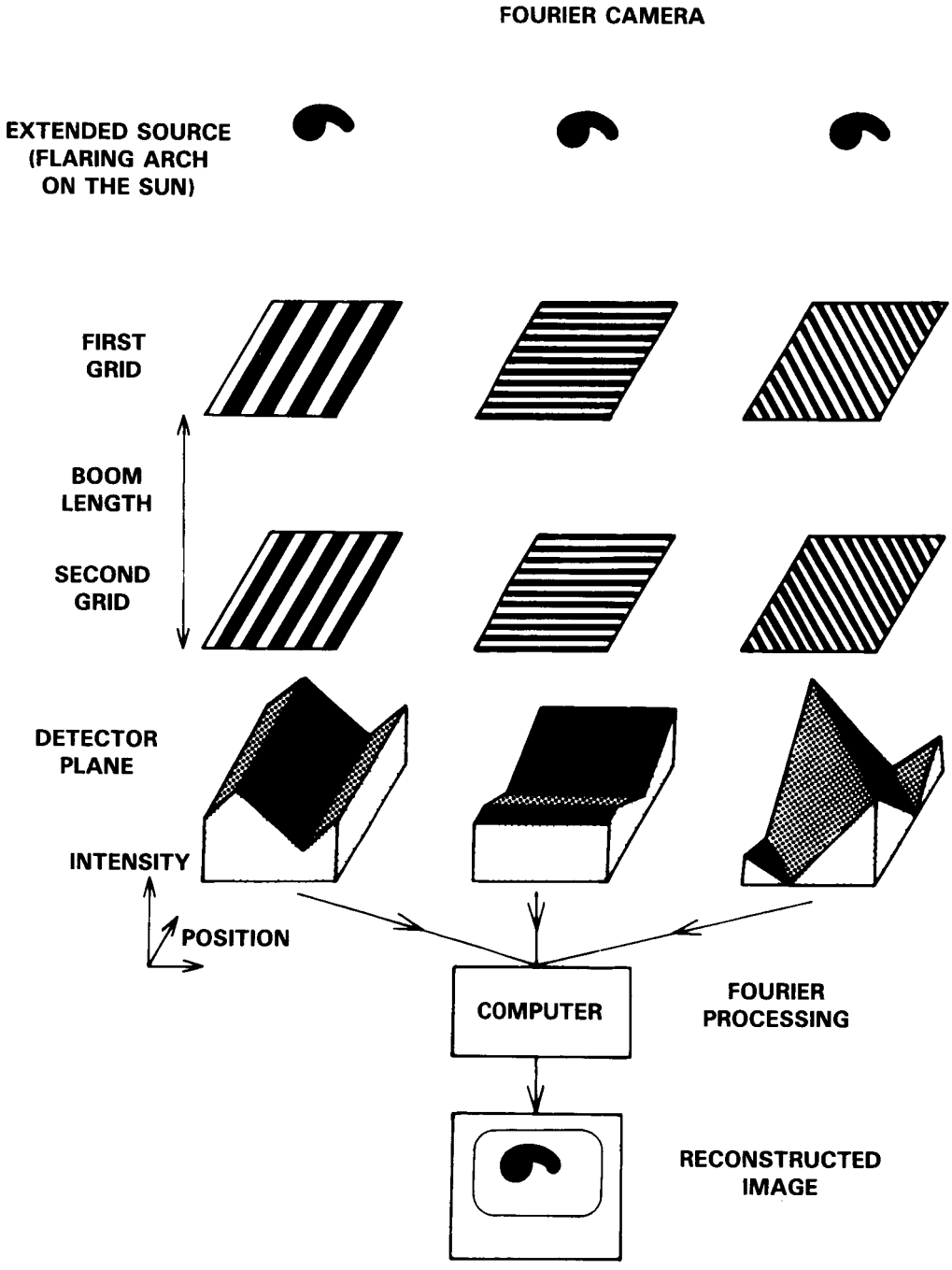

Figure A.1. Schematic of the Fourier-transform imaging technique.

A1.3. Aspect System

The high-resolution imaging instruments planned for this mission require a spacecraft pointing capability of arcsecond accuracy. In addition, operation of **GRID** requires knowledge of the position of the grids at the outer end of the boom with respect to the grids mounted on the spacecraft. Both of these requirements can be satisfied by use of a modified version of the **SDS**, an instrument designed to obtain precise measurements of the solar diameter.

The operating principles of **SDS** are illustrated in Figure A.2. The primary optical element used to form multiple images of the Sun is a stable, partially transmitting beam-splitting wedge of precisely known angle. A long-focal-length telescope is used to image the first two of the series of solar images onto a set of linear arrays placed in the focal plane. As implemented for the **MAX '91** mission, the beam-splitting wedge will be combined with a refractive lens of focal length 6·8 m. This combination mounted on the outer end of the boom will produce images at the base of the boom, where the linear array detectors are mounted in precise placement with respect to the inner grids.

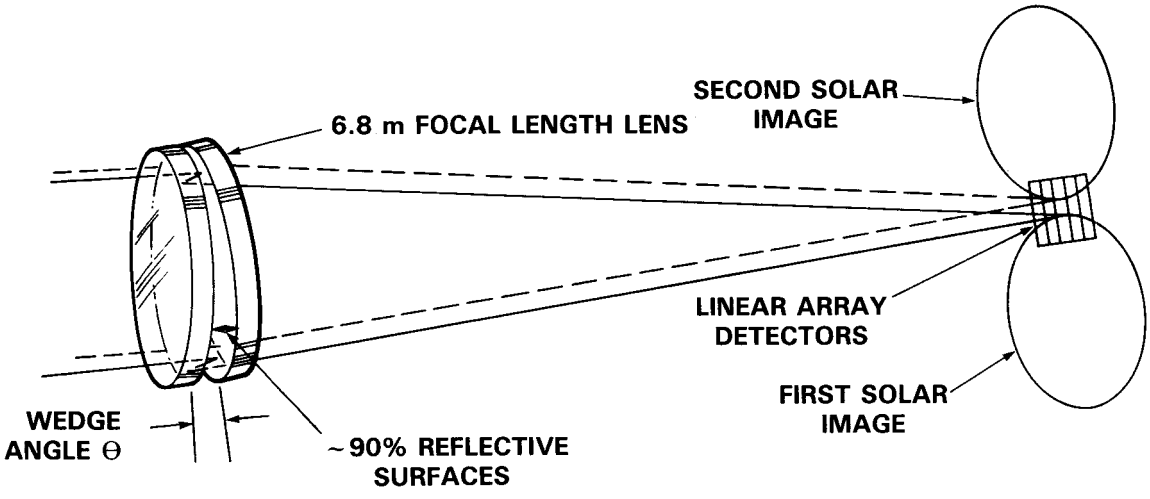

Figure A.2. Schematic showing the operating principles of **SDS**. Note that the wedge angle θ is set to approximately half the solar diameter or ~990 arcseconds.

Two **SDS**s will be required to establish the relative roll alignment of the inner and outer sets of grids to 1 arcsecond (Figure 3.2). The real-time system will determine the position of each of the solar edges viewed by the detectors. From the sets of edge positions, the location of the centers of the solar images will then be computed. The position in the image plane of the center of the first solar image can then be algebraically compared with the previously established desired position of the image center to provide the desired spacecraft fine-pointing error function. In addition to providing aspect information for **GRID**, the two **SDS**s will measure perpendicular solar diameters simultaneously and with sufficient precision to provide substantial scientific return in their own right (see discussion in Section 3.5).

APPENDIX 2. HIGH RESOLUTION GAMMA RAY AND NEUTRON SPECTROMETER (HIGRANS)

HIGRANS consists of an array of high-resolution HPGe detectors in a BGO scintillator annulus and back shield/detector assembly (see Figure 3.4). The detector system is enclosed in a plastic-scintillator charged-particle shield. The HPGe detectors are contained in a single cryostat and cooled to an operating temperature of 90 K with a two-stage solid-cryogen (methane/ammonia) refrigerator via a cold finger.

The array of HPGe detectors is made up of 12 segmented n-type detectors (6 cm diameter $\times$ 6 cm thick) operating over an energy range of 10 keV to 100 MeV. N-type material was chosen to minimize detector degradation from long-term exposure to energetic particles in space. Each detector has a closed-end coaxial geometry and is electrically segmented into a 1·5-cm-thick front section and a 4·5-cm-thick rear section (Figure A.3). The segmentation provides optimal signal-to-background over the entire energy range from about 10 keV to 100 MeV for photons incident on the front face of the detector.

Photons below about 200 keV are stopped primarily by photoelectric absorption in the front segment, while background is rejected by anticoincidence with the rear segment. The front segment has substantially lower capacitance than a normal planar detector of the same dimensions, resulting in state-of-the-art energy resolution. γ-Rays above about 200 keV interact primarily via Compton scattering and pair production and thus tend to deposit energy in multiple sites in the detector. The dominant background in a well-shielded detector at energies between 200 keV and 2 MeV is the β-decay of proton- and neutron-induced radionuclides in the HPGe detector. These β-decays deposit energy at a single site because of the short range of the β-particle. Front-rear coincidences and pulse-shape discrimination in the rear segment are used to identify and separate multiple-site from single-site interactions in the HPGe detector and so minimize this source of background.

The 5-cm-thick shield annulus and the three rear sections are composed of a matrix of BGO units, each with its own photomultiplier tube, preamplifier, discriminator, high-voltage power supply, LED light pulser, and servo-gain-control electronics. The BGO assembly performs several functions. At energies below 20 MeV, the assembly provides active collimation and shielding for the HPGe array against γ-ray background. The annulus and first rear section also reject γ-rays which are Compton scattered in the HPGe and deposit energy in the BGO above the shield threshold level. This makes the instrument response matrix more nearly diagonal, permitting more accurate determination of the incident photon spectrum. At energies above 20 MeV, the three back sections together with the HPGe array form a multilayer high-energy γ-ray and neutron spectrometer. The relative energy loss in these layers can be used to differentiate between events produced by γ-rays and neutrons. The improvement in the neutron sensitivity of **HIGRANS** compared with that of **GRS** is a factor of 10 or more (Figure A.4). The sensitivity to γ-rays above 20 MeV shows a similar improvement of a factor of 5 or more. The upper layer of the rear shield is also pulse-height analyzed over the energy range from 100 keV to 20 MeV, thus complementing the HPGe data with high photofraction measurements of broad lines and the continuum. The charged-particle 4π steradian shield consists of a dome and a rear section fabricated from low-light-loss plastic scintillator such as NE110 and viewed with photomultiplier tubes.

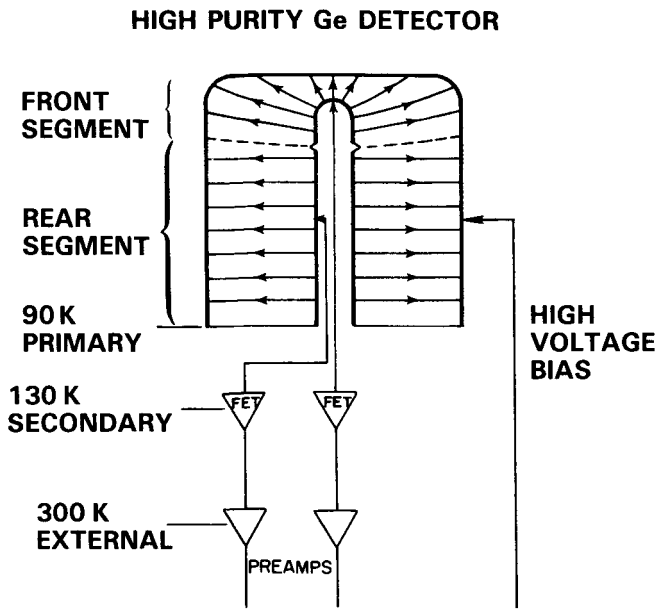

Figure A.3. Concept of a segmented HPGe detector.

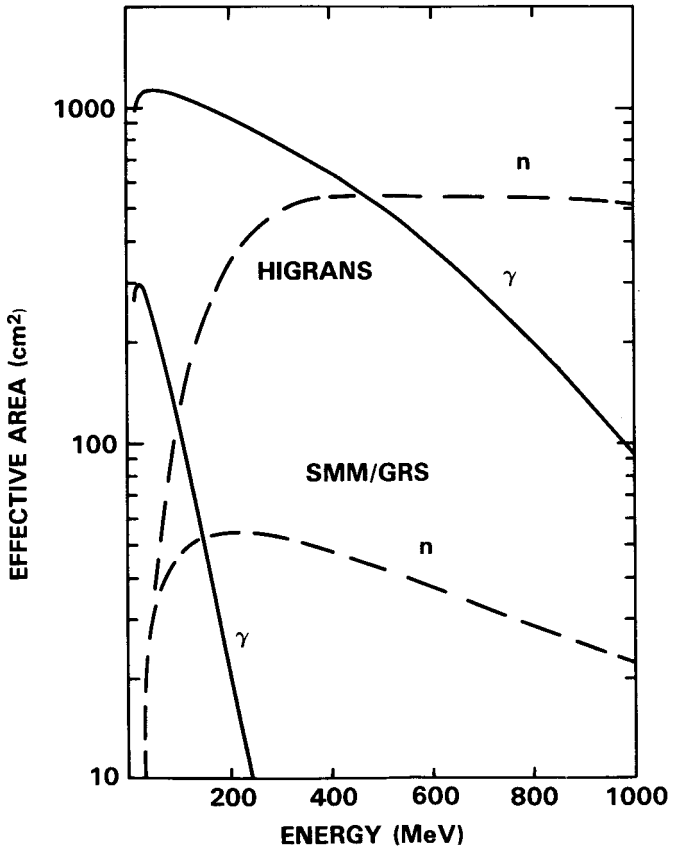

Figure A.4. Calculated effective area of **HIGRANS** compared with **GRS** for high-energy γ-rays (solid lines) and neutrons (dashed lines).

APPENDIX 3. LOW ENERGY IMAGER (LEI)

A3.1. Soft X-Ray/UV Polychromatic Imaging System (XUVIS)

This is a high-resolution instrument package, designed to study solar plasmas with temperatures ranging from the temperature minimum to about 2×10^7 K. It includes two optical trains, one for the UV and one for soft X-rays. Both optical systems use array detectors of the same type, so that the development cost for the detector electronics system occurs only once. The command and data system, common to both optical trains, is microprocessor controlled, so that data from the X-ray system may be used to optimize the observing mode of the UV optical system and vice versa.

The illustrated soft X-ray optical system (Figure A.5) is based on an existing Wolter Type I telescope remaining from the **Skylab** program. It uses a series of small multilayer tertiary mirrors to isolate individual spectral lines, so that each image is for a well-defined temperature range. The multilayer coating on each mirror acts like an artificial Bragg crystal, preferentially reflecting radiation whose wavelength satisfies the Bragg condition at normal incidence. In addition to providing wavelength discrimination, the tertiary mirrors magnify the primary image formed by the Wolter I system, so that the final image scale matches the pixel size of the array detector. The tertiary mirrors may be mounted on a rotating turret, permitting different sets of lines to be selected. Up to four tertiary mirrors may simultaneously share the primary beam, forming their images on a common detector located on the optical axis of the main telescope. Metal-coated thin-plastic-film filters will be used to exclude UV, visible, and near-infrared radiation.

The UV optical system (Figure A.5) is designed around the spectrometer portion of the **UVSP**, which will become available when **SMM** is retrieved from orbit. The optomechanical system of **UVSP** will be retrofitted with a new telescope of longer focal length to increase both the aperture area and the plate scale. The spectrometer features an Ebert-Fastie optical system, while the telescope is of the Gregorian configuration. Use of a field stop at the prime focus of the telescope limits the flux level on the secondary and captures the bulk of the heat load of the incoming solar flux. Articulation of the telescope optics will permit the UV system to observe anywhere on the solar disk. Use of an array detector rather than separate photomultipliers makes the system effectively 1000 times faster than the current **UVSP**. An array detector has an additional advantage in that it is capable of electronically shifting its stored charge image in synchronization with other activities in the instrument, such as moving the telescope line of sight across the Sun. Since the spectrometer is essentially stigmatic, a relatively long entrance slit can be used, and points on the Sun will map onto points along the images of spectral lines in the final focal plane. Assuming a 1000 x 1000 array detector, the spectrometer will accept a 40 Å interval that can be set anywhere in the 1200- to 1800-Å spectral range. Interchangable masks in the spectrometer focal plane, together with the image-shifting capability of the array detector, allow the instrument to operate in a variety of modes according to the requirements of the observing program. The system can function as a simplex spectrograph, a multislit spectrograph, a Doppler camera, a high-speed line-profile polychromator, or a streak camera.

In addition to collecting primary data for plasma diagnostics, the UV system can provide a flare alert function, since the onset of a flare tends to show up first in transition zone lines such as C IV. The observing mode for a flare watch will consist of a cyclic survey of all active regions

on the disk, with the locations of the regions being defined using the soft X-ray optical system. Each observing cycle will last only a few seconds, with the brightest point in each region being retained in memory. A sudden increase in the intensity of one of the bright points defines flare onset. Upon detection of the onset of a flare, the control microprocessor will transmit a flare alert to to other instruments in the observatory.

Provisional Specifications for the UV Spectrometer System

•Aperture Area:	1050 cm^2 (total collecting area) 50 cm^2 (effective area including efficiency)
•Stigmatic Spectrograph Mode:	5-arcminute slit length 40-Å interval in range 1200 to 1800 Å 0.04-Å resolution elements 0.3 to 1 s time resolution
•Spectroheliograph Mode:	5 × 5 arcminute field of view any spectral line in range 1200 to 1800 Å (line intensity only – no profile) 0.3 to 1 s time resolution for full field
•Streak Camera Mode:	slit, 5 arcminute long, fixed in position on Sun 0.5-arcsecond pixels along slit any spectrum line in range 1200 to 3000 Å (line intensity only) 6 to 10 ms time resolution
•Multiple Slit Mode:	10 to 20 parallel slits usable at C IV full line profiles 0·3 to 1 s time resolution
•Dopplergram Mode:	5-arcminute-long slit full line profiles velocity range ± 400 km s^{-1} 10 slit positions per second time resolution: 60 s for 5 × 5-arcminute field 12 s for 1 × 5-arcminute field

Provisional Specifications for the Soft X-ray Imaging System

•Effective Aperture:	1 to 2 cm^2 (total)
•Bandwidth:	3 Å (typical at 95 Å)
•Field of View:	2000 × 2000 arcseconds
•Pixel Size:	1 × 1 arcsecond
•Time Resolution:	
•Nominal Mode	1 s
•Streak Mode	0·2 to 10 ms
•Monochromatic Mode	10 s
•Dynamic Range:	10^5 (CCD 5000, exposure time 20 s)
•Temperature Coverage:	5×10^5 to 2×10^7 K

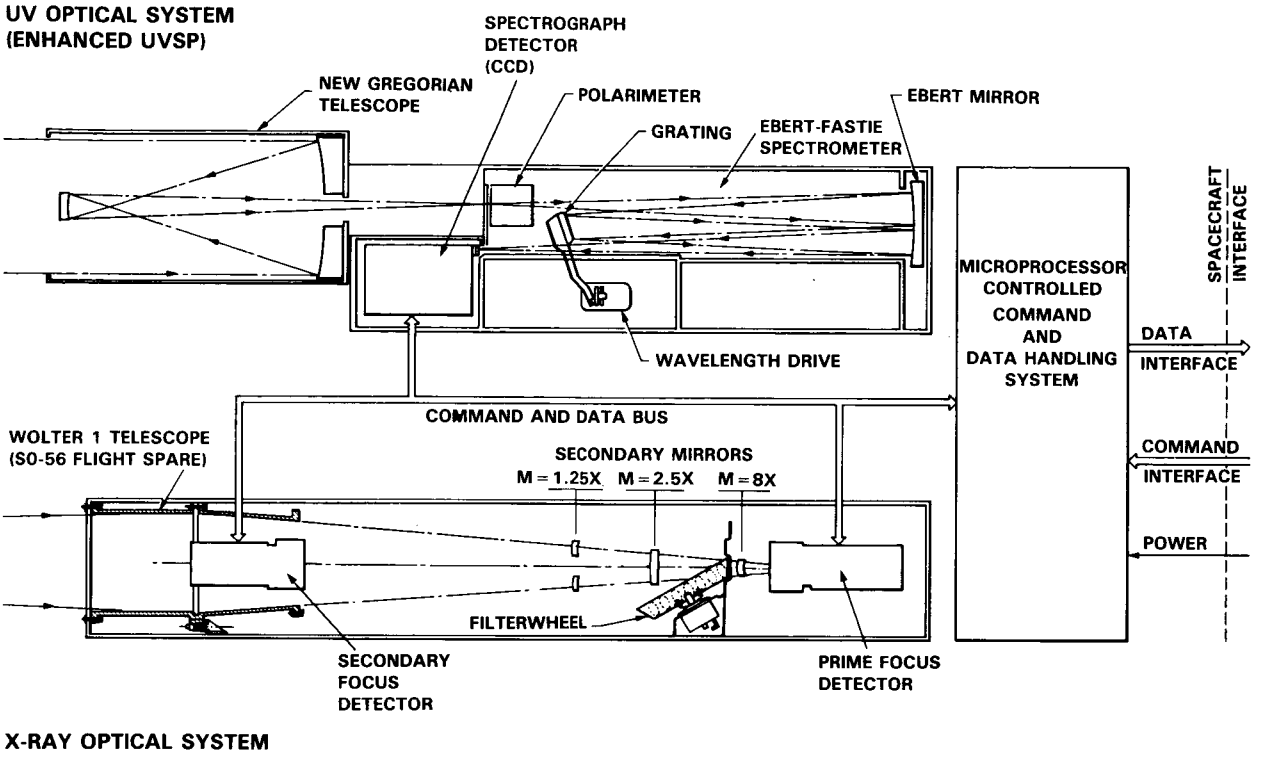

Figure A.5. The Soft X-Ray/UV Polychromatic Imaging System.

A3.2. Soft X-Ray Polychromatic Imaging Experiment

This instrument is a high resolution soft X-ray imaging system based on the use of normal-incidence multilayer mirrors. A possible system is shown in Figure A.6. This instrument concept is at least 10 times as sensitive as the X-ray imaging system based on the **Skylab** Wolter Type I telescope described in Appendix 3.1 and could be substituted for the latter in the **MAX '91** payload at a comparable cost.

Multilayer mirror coatings, also known as layered synthetic microstructures (LSMs), consist of alternating layers of high- and low-Z materials such as tungsten and carbon, respectively. The thicknesses of the layer pairs are adjusted such that the Bragg condition for X-ray diffraction is satisfied at normal incidence for a desired X-ray wavelength. The high-Z layers play the role of the crystal planes in ordinary X-ray diffraction, while the low-Z layers serve to define the separation of the artificial crystal planes and, hence, the wavelength at which they reflect. The bandwidth of the coating is roughly given by the design wavelength divided by the number of

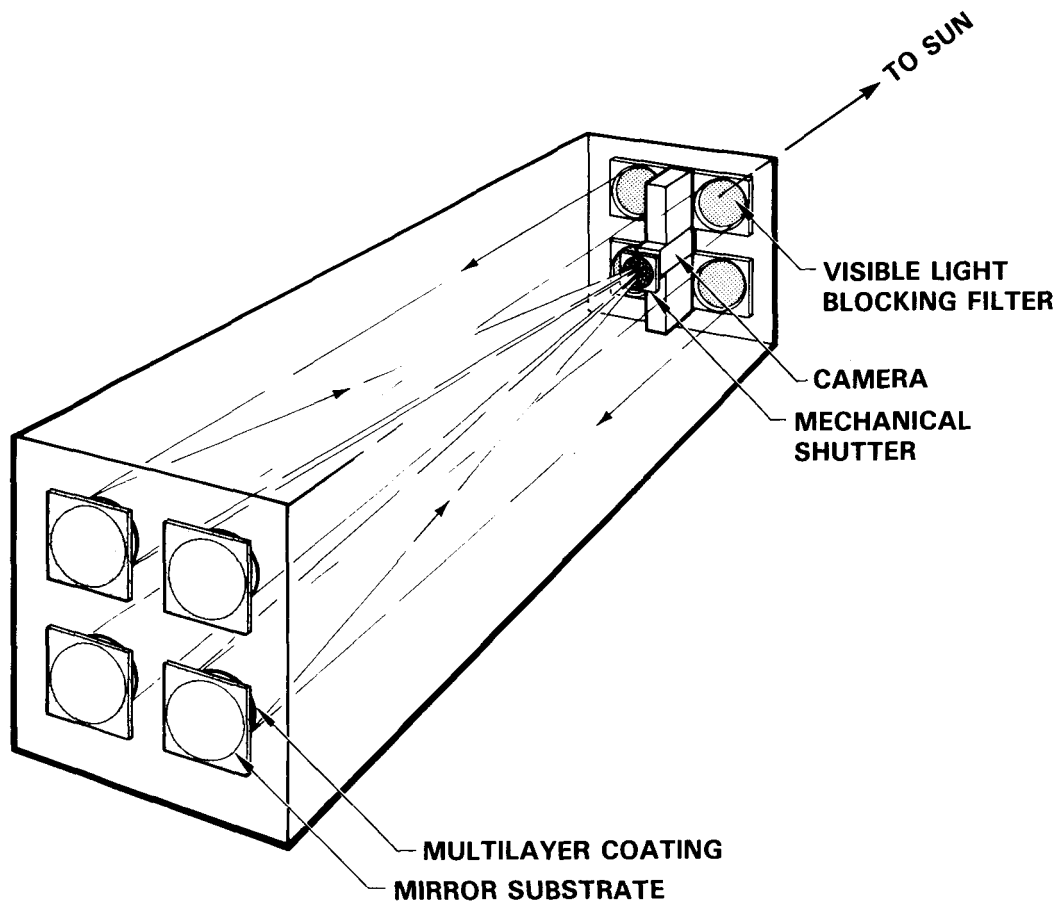

Figure A.6. Schematic of a four channel, soft X-ray imaging system using multilayer, normal incidence mirrors.

layer pairs. Efficiencies range from a few percent to about 50%, depending upon the design wavelength.

The design concept for the imaging polychromator instrument is based on normal incidence prime focus optics. This approach has the advantages of superior imaging, large field of view, large aperture, high efficiency, ease of manufacture, low sensitivity to optical misalignments, and low cost relative to other alternatives. The narrow passbands characteristic of multilayer coatings allow the isolation of strong lines to give each channel of the system a response to plasma over a well defined temperature range.

The system illustrated in Figure A.6 features four channels covering wavelengths between 44 and 184 Å, and temperatures between 5×10^5 and 10^7 K. Other lines in the same general wavelength range can be substituted, extending the upper temperature limit to 2×10^7 K. The four channels share a single detector, with the fields of view overlapping but displaced from one another so that bright regions can be observed simultaneously at the different wavelengths during the impulsive phase. A monochromatic mode, in which only one wavelength at a time

is observed, allows the full structure of the flare loop system to be observed without overlap during the gradual phase. For very high time resolution, a streak camera mode is provided in which the array detector counts are continuously shifted out while the exposure is being made. Each flaring point will leave a streak on the image, and rapid variations of the point brightness will be revealed as variations in image brightness along the streak. Time resolution in the streak mode can be in the millisecond range, even though the total framing rate is only one frame every few seconds. Use of a shared detector minimizes both total system cost and the total data rate that must be accommodated by the telemetry system.

The large format CCD array detector is presently in the development stage. An alternative detector system, containing off-the-shelf components, employs a fine-grain phosphor coupled to a very high resolution TV tube (Plumbicon) via an image intensifier. This system has a resolution of > 2500 lines and has been demonstrated to be capable of 2 μm pixels at the focal plane, in contrast to the 27 μm pixels of the CCD. Instead of a 5 m focal length, the instrument would be shortened to 2 m and employ a 10 μm pixel, well within the detector's resolution. In flare mode, a portion of the full image is scanned at a time resolution of a few milliseconds. This system represents a modern version of the type typified by the EUV monitor flown on **Skylab** as part of the **S082** experiment.

Broad science goals for the imaging polychromator are the determination of geometrical and radiating properties of coronal plasmas in the temperature range from 5×10^5 to 2×10^7 K, including the geometry and its evolution, the plasma properties and their spatial variation, the energetics and the total radiated power, and the dynamics of loop formation. The instrument will provide boundary conditions for the interpretation of data from nonimaging instruments, including the locations and sizes of flare footpoints, and the sizes, shapes, and orientations of flare loop systems. Another objective is to observe the short-term evolution of the soft X-ray plasma during the impulsive phase.

Instrument design goals for the imaging polychromator include high spatial resolution (1 arcsecond pixels), whole-Sun coverage, high time resolution (milliseconds to seconds), high photometric sensitivity, well-defined temperature sensitivity, a simple design to minimize cost, multiple operating modes, and a versatile microprocessor controlled command and data handling system.

Provisional Specifications for the Soft X-Ray Imaging Polychromator

•Effective Aperture:	2.5 - 10 cm^2 per channel
•Bandwidth:	3 Å at 95 Å; 1 Å at 49 Å; 20 Å at 180 Å
•Field of View:	2000 × 2000 arcseconds
•Pixel Size:	1 × 1 arcsecond
•Time Resolution:	
Nominal Mode	1 s
Streak Mode	0·2 to 10 ms
Monochromatic Mode	10 s
•Dynamic Range:	10^5
•Temperature Coverage:	5×10^5 to 10^7 K

A3.3. EUV Spectrograph/Spectroheliograph

This instrument will provide stigmatic spectral images with high spatial and spectral resolutions at EUV wavelengths between 240 and 470 Å. Quantitative information on solar plasmas ranging from the lower transition zone at temperatures of about 5×10^4 K to the thermal components of flares at temperatures as high as 2×10^7 K will be obtained with this instrument. The EUV spectral range is unique in that it provides thorough coverage of this very important temperature regime within a relatively narrow band of wavelengths. A large number of close line pairs in the EUV provide useful spectroscopic diagnostics in the temperature and density ranges characteristic of flare and preflare plasmas. Thus, observations in this spectral region allow the determination of the electron densities, differential emission measures, mass flows, and nonthermal random mass motions (turbulence) throughout the observed solar features. The simultaneous high spatial and spectral resolution of this instrument mean that line profiles measured with it will give the mass flows and random mass motions of well defined solar plasmas through Dopppler shifts and Doppler broadenings. Combined with the ability to observe high-temperature lines (e.g., Fe XXIV 255 Å and Fe XXIII 263 Å), the spatial and spectral capabilities of this instrument will permit detailed mapping of the temperature/density structure of flare loops.

One possible concept for such an EUV instrument is based on the **SEUTS** design which had been selected for flight on **Spacelab** but was subsequently cancelled. A set of spectrograph optics and a nearly completed telescope have already been made for that project and thus are currently available hardware. In addition, a substantial amount of design and analysis has been done on the instrument as a whole, which would be directly applicable to a version of the instrument suitable for inclusion on the **MAX '91** mission.

The **SEUTS** design shown in Figure A.7 combines a Wolter Type II grazing-incidence telescope having high EUV reflectance with an aspheric near-normal-incidence grating system, which produces nearly stigmatic images of the solar atmosphere at each wavelength. A slit placed at the focus of the telescope simultaneously acts as the entrance aperture for the spectrograph and defines the array of spatial elements that will be refocussed at each wavelength onto the surface of an array detector. This optical design also provides considerable operational flexibility via commandable selection of entrance apertures and detector read-out modes. This flexibility can be employed to optimize scientific observing programs.

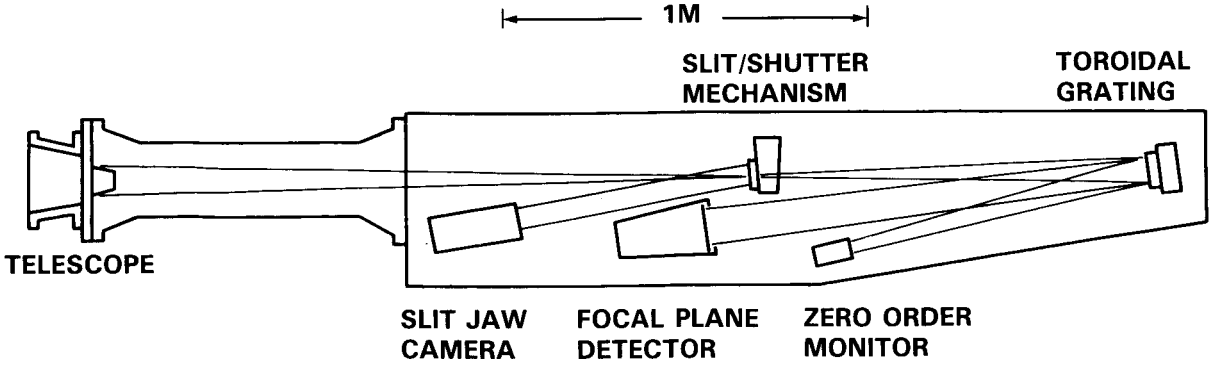

Figure A.7. Schematic showing the optical layout of the **SEUTS** instrument.

The present **SEUTS** baseline design incorporates the following:

- A line-profile mode yielding stigmatic spectra (with resolution elements of 0.02 Å) over the 8-arcminute length of the entrance slit. In this mode the instrument will produce spectra in the range from 240 to 470 Å while maintaining unambiguous spatial information perpendicular to the spectral dispersion plane.
- A nonoverlapping spectroheliogram mode with a 0.3 × 8 arcminute field of view for many strong lines. The slit width of 20 arcseconds corresponds spectrally to about 1Å, so that non-overlapping solar images are formed simultaneously at most of the detected wavelengths. A wider field of view can be built up by shifting the image 20 arcseconds between observations.
- A combination mode providing spectroheliograms over most of a 0.3 × 8 arcminute field of view but with line profile observations in the central (48-arcsecond) portion of the field.
- A fast timing mode in which only a few selected columns of the array detector are repeatedly read out, providing extremely high time-resolution measurements of the intensity variations in strong emission lines at each position along the 8-arcminute length of the entrance slit.
- A wide field mode (5 × 8 arcminute field of view) for flare studies, with spatial resolution in the direction of dispersion governed by the Doppler widths of the spectral lines. In this mode, the instrument is similar to the **S082A** slitless spectrograph on **Skylab**.

The overall instrumental performance and dimensions are summarized below:

- Wavelength range: 240 to 470 Å
- field of view: 8 arcminutes × 0·5 arcseconds in line-profile mode
  8 × 5 arcminutes in wide-field mode
- Spatial resolution: 1·3 arcseconds (best); 2·0 arcseconds (typical)
- Spectral resolution: 0·02 Å (best); 0·03 Å (typical)
- Temporal resolution: 1 s in line-profile and spectroheliogram modes
  30 ms in fast timing mode
- Telescope aperture: 150 cm^2 geometric area
  46 cm^2 effective area at 300Å
- Physical envelope: 325 × 60 × 30 cm
- Total weight: 130 kg

Another way to achieve an EUV capability on **MAX '91** would be to use a modified **SERTS** instrument, which is the sounding rocket version of **SEUTS**. That instrument (an engineering success on its one flight to date) has the same spectrograph section but a somewhat smaller telescope than **SEUTS**, thus reducing the length and weight of the overall instrument package. A **SERTS**-sized instrument would have the same spectral performance and operating modes as listed above, but would trade poorer spatial resolution (about 3 arcseconds) for a larger field of view (10 × 16 arcminutes). Such an instrument modified for the **MAX '91** mission would also be able to utilize a considerable amount of existing hardware.

APPENDIX 4. SOFT X-RAY IMPULSIVE PHASE SPECTROMETER (SIPS)

The **SIPS** spectrometers referred to in Section 3.4 will be used to study the dynamics of the impulsive phase of flares, and to determine important plasma parameters, such as electron temperature, differential emission measure, and ionization balance. They also will be used to measure absolute abundances for many elements, including relatively rare elements (e.g., Ar, K, and Mn). The improved sensitivity of **SIPS** will allow line profile measurements to be made on time scales of about 1 s with **HSFCS**, and temperature and velocity diagnostics on time scales of 1 to 3 s with **HSBCS**.

The mechanical structure for the **HSBCS** will be largely identical to that of the **BCS**. It will consist of eight curved crystal assemblies and eight corresponding one-dimensional position sensitive proportional counters. An attractive feature of the bent-crystal design is that it requires no moving parts and thus is highly reliable. The multiplicity of similar channels also adds redundancy as well as sensitivity. The major difference between the designs of the **HSBCS** and the **BCS**will be the omission of the 6-arcminute FWHM collimator. Not only will this make possible whole-Sun viewing without the need to point the spacecraft, but it will also increase the instrument sensitivity by about a factor of 3.

HSFCS will be a conventional scanning Bragg crystal spectrometer. The design will be a greatly improved version of the **P78-1** spectrometer (**SOLFLEX**). The two **HSFCS** crystals are independently driven and will have effective areas about 6 times greater than than those of the **SOLFLEX** spectrometers. The **HSFCS** spectrometers will scan any selected wavelength range between 1 and 10 Å. This complete range can be scanned in about 5 minutes.

HSBCS will use germanium crystals with the same two cuts as used for the **BCS**. These crystals can be easily bent and provide high spectral resolution and reflectivity. Other crystals with higher reflectivity and spectral resolution also will be considered. One of the **HSFCS** spectrometers will include a germanium crystal to provide in-orbit cross-calibration of wavelength dispersion with **HSBCS**. The 1-10 Å **HSFCS** channel will use an ADP crystal.

The **HSBCS** detectors will be sealed, one-dimensional position-sensitive proportional counters. The position resolution of the detectors will be increased fourfold over the **BCS** by making use of a modified wedge and strip design for the readout. The double wedge readout provides low thermal noise, low distortion, and good linearity. **HSFCS** will use two standard sealed proportional counters, and thus, require no gas supply system.

The design of the digital electronics will be based on the design of the **BCS** electronics and will use the same microprocessor (an RCA 1802). The present software will be adapted for the increased capabilities of the **HSBCS**. The power supply system would be similar to that of the **BCS**. The microprocessor adds flexibility to the instrument, making it possible to vary the temporal and spectral resolution of the different channels, coordinate flare observations between the two spectrometers, and optimize the overall performance. Alternatively, the data can be processed at a higher rate and put in a queued memory store for later transmission; this can improve the time resolution by at least a factor of 2 in all channels during the impulsive phase. The microprocessor makes possible in-orbit software modifications, real-time processing of the data, and flare alerts to other instruments on board. Much of the analysis software developed for **XRP** can be directly adapted for use with **SIPS** data, thus achieving equivalent savings to that obtained by using existing mechanical and electronic designs.

BIBLIOGRAPHY

Scientific Considerations

Energetic Phenomena on the Sun, Proceedings of the SMM Workshops, M. Kundu and B.E. Woodgate, eds., to be published as a NASA CP, 1986.

Solar Flares, A Monograph from the Skylab Solar Workshop II, P.A. Sturrock, ed., Colorado Assoc. Univ. Press, 1980.

The Sun as a Star, S. Jordan, ed., Monograph Series on Nonthermal Phenomena in Stellar Atmospheres, NASA SP-450, 1981.

Physics of the Sun, P.A. Sturrock, ed., Geophysics and Astrophysics Monographs, D. Reidel Publishing Co., 1986.

GRID

Fourier-Transform Imaging for X-Ray Astronomy, G.J. Hurford and H.S. Hudson, Big Bear Solar Observatory report # 1080, UCSD report # SP-79-27, 1979.

A Fourier-Transform Telescope for Sub-arcsecond Imaging of X-rays and Gamma-Rays, C.J. Crannell, G.J. Hurford, L.E. Orwig, and T.A. Prince, Proc. Soc. Photo-Optical Engineers, 1986.

Solar Disk Sextant, S. Sofia, H. Chiu, E. Maier, K. Schatten, P. Minott, and E. Endal, Applied Optics, *23*, 1226, 1984.

HIGRANS

High Energy Neutral Radiations from the Sun, E.L. Chupp, Ann. Rev. Astron. Astrophys., *22*, 359, 1984.

A New Component of Hard X-Rays in Solar Flares, R.P. Lin, R.A. Schwartz, R.M. Pelling, and K.C. Hurley, Ap. J., *251*, L109, 1981.